

Open access • Posted Content • DOI:10.1101/2020.02.24.962902

RNF40-dependent epigenetic regulation of actin cytoskeletal dynamics is required for HER2-driven mammary tumorigenesis — Source link ☑

 Florian Wegwitz, Evangelos Prokakis, Pejkovska A, Robyn Laura Kosinsky ...+6 more authors

 Institutions: University of Göttingen, University of Hamburg, Mayo Clinic

 Published on: 25 Feb 2020 - bioRxiv (Cold Spring Harbor Laboratory)

 Topics: Monoubiquitination, Actin cytoskeleton, Epigenome, Ubiquitin ligase and Breast cancer

Related papers:

- The histone H2B ubiquitin ligase RNF40 is required for HER2-driven mammary tumorigenesis.
- Role of RNF20 in cancer development and progression a comprehensive review
- RNF6 as an Oncogene and Potential Therapeutic Target—A Review
- Two-faced activity of RNF8: What "twists" it from a genome guardian to a cancer facilitator?
- The Functions of DNA Damage Factor RNF8 in the Pathogenesis and Progression of Cancer.

Share this paper: 😗 🄰 🛅 🖂

1 Title

2 RNF40-dependent epigenetic regulation of actin cytoskeletal dynamics is required for HER2-driven mammary

- 3 tumorigenesis
- 4

5 Authors and affiliations

6 Florian Wegwitz^{1,*}, Evangelos Prokakis^{1,*}, Anastasija Pejkovska¹, Robyn Laura Kosinsky¹, Markus Glatzel², Klaus

7 Pantel³, Harriet Wikman³, Steven A. Johnsen^{1,3,4,#}

- 8
- 9 ¹Department of General, Visceral and Pediatric Surgery, University Medical Center Göttingen, Göttingen,
- 10 Germany
- ²Institute for Neuropathology, University of Hamburg-Eppendorf, Hamburg, Germany
- ¹² ³Institute of Tumor Biology, University Medical Center Hamburg-Eppendorf, Hamburg, Germany
- ⁴Gene Regulatory Mechanisms and Molecular Epigenetics Lab, Division of Gastroenterology and Hepatology,
- 14 Mayo Clinic, Rochester, MN, USA
- 15
- 16 *These authors contributed equally to this work
- 17 [#]Address correspondence to <u>johnsen.steven@mayo.edu</u> (S.A.J.)
- 18
- 19 Running title
- 20 RNF40 controls RHO-ROCK signaling in HER2-driven breast cancer
- 21
- 22 Keywords
- 23 RNF40, H2Bub1, actin, ROCK1, cancer

- 25 This work was supported by funding from the Deutsche Krebshilfe to S.A.J. (111600), and to H.W. and K.P.
- 26 (Priority Program "Translational Oncology"; 70112507).
- 27

28 CORRESPONDING AUTHOR INFORMATION

- 29 Steven A. Johnsen, Ph.D.
- 30 Division of Gastroenterology and Hepatology
- 31 Mayo Clinic
- 32 200 First St SW
- 33 Rochester, MN 55902
- 34 Tel.: +1 507 255-6138
- 35 Fax: +1 507 255-6318
- 36 Email: johnsen.steven@mayo.edu
- 37
- 38 **Conflict of interest**
- 39 F.W., E.P., A.P., R.L.K., K.P., H.W., M.G. and S.A.J. declare no conflict of interest.

- 41
- 42

43 Abstract

The HER2-driven breast cancer subtype displays a particularly aggressive behavior. Alterations of the epigenome 44 45 are common in cancers and represent attractive novel molecular therapeutic targets. Monoubiquitination of 46 histone 2B (H2Bub1) by its obligate heterodimeric E3 ubiquitin ligase complex RNF20/RNF40 has been described 47 to have tumor suppressor functions and loss of H2Bub1 has been associated with cancer progression. In this 48 study, we utilized human tumor samples, cell culture models, and a mammary carcinoma mouse model with 49 tissue-specific Rnf40 deletion and identified an unexpected tumor-supportive role of RNF40 in HER2-positive 50 breast cancer. We demonstrate that RNF40-driven H2B monoubiquitination is essential for transcriptional 51 activation of RHO/ROCK/LIMK pathway components and proper actin cytoskeleton dynamics through a trans-52 histone crosstalk with histone 3 lysine 4 trimethylation (H3K4me3). Collectively, this work demonstrates a 53 previously unknown essential role of RNF40 in HER2-positive breast cancer, revealing the RNF20/RNF40/H2Bub1 54 axis as a possible tumor context-dependent therapeutic target in breast cancer.

55

56 Statement of significance

57 HER2-positive breast cancer patients frequently develop resistance to anti-HER2 therapies. Here we 58 demonstrate that RNF20/RNF40-mediated H2B monoubiquitination supports the oncogenic properties of cancer 59 cells of this subtype by regulating actin dynamics. The RNF20/RNF40/H2Bub1 axis may therefore represent an 60 attractive drug target for novel therapies.

62 Introduction

63 Breast cancer (BC) is the most common form of cancer in the female population (1). The survival rates of BC vary 64 greatly and strongly depend upon both early detection as well as the molecular subtype (2). Breast cancer can 65 be separated into at least four distinct molecular subtypes based on the expression of the estrogen receptor 66 (ER), progesterone receptor (PR) or human epidermal growth factor receptor 2 (HER2) receptor. Notably, the 67 HER2-positive and triple negative (HER2-, ER-, PR-) BC subtypes are generally more invasive and display a poorer 68 prognosis compared to hormone receptor-positive (ER+ or/and PR+) BC (3). Importantly, while current anti-69 HER2 therapies are initially highly effective for many BC patients with HER2-positive tumors, a significant 70 number of patients develop tumors refractory to therapy and display tumor relapse and disease progression (4). 71 Thus, new approaches are necessary to combat HER2-positive breast cancer.

72 Precision oncology approaches aim to utilize or develop novel targeted therapies which exploit tumor-specific 73 dependencies and/or vulnerabilities based on specific molecular alterations present in a given tumor or 74 molecular subtype (5). In addition to genetic alterations that occur in cancer, a large body of emerging evidence 75 has demonstrated the additional importance of epigenetic alterations in tumorigenesis and tumor progression. These alterations can occur either through the direct mutation of genes encoding epigenetic regulatory proteins 76 77 or as secondary events downstream of signaling pathways altered as a result of other genetic changes (6). These 78 changes can result in altered patterns of DNA methylation, post-translational histone modifications, and changes 79 in chromatin accessibility or chromatin architecture. Due to the reversible nature of many of these changes, 80 numerous substances are currently in various stages of pre-clinical and clinical testing to determine their 81 efficacy as anti-cancer therapies (7).

Previous work from our lab and others revealed a particular importance of histone 2B monoubiquitination (H2Bub1) in controlling cellular differentiation (8–10) and demonstrated that H2Bub1 levels are decreased in ERpositive BC compared to normal adjacent epithelium (11,12). These findings have led to the hypothesis that H2Bub1, catalyzed by the obligate heterodimeric Ring Finger Protein 20 and 40 (RNF20/RNF40) E3 ubiquitin ligase complex, has a tumor suppressive function. This hypothesis has been further supported by studies

investigating the function of RNF20 and RNF40 (13–17). In contrast, we and others have uncovered tumor
supportive roles of RNF20 and RNF40 in colorectal cancer (18,19) and androgen-dependent prostate cancer (20).
Therefore, together these findings suggest that RNF20/RNF40-driven H2B monoubiquitination plays a contextdependent role in cancer.

91 At the molecular level, H2Bub1 is localized across the body of active genes (21) and is closely coupled to 92 transcriptional elongation (22–25). Studies in both yeast and human cells have revealed a particular coupling of 93 H2Bub1 and the trimethylation of lysines 4 and 79 of histone 3 (H3K4me3 and H3K79me3, respectively) near the 94 transcriptional start site and transcribed regions, respectively, of active genes (22,26-30). Past studies have 95 reported an extension of H3K4me3 into the transcribed region of genes displaying a particularly high 96 transcriptional elongation rate (31), as well as a close link between H2Bub1 and transcriptional elongation (23). 97 Consistently, we recently demonstrated that loss of RNF40-mediated H2B monoubiguitination results in the 98 narrowing of H3K4me3 domains near the transcriptional start site (TSS) of important cell fate-determining genes 99 displaying high elongation rates (22).

100 In this study we sought to examine the role of RNF40-mediated H2B monoubiquitination in the HER2-driven 101 subtype of BC. Our studies using a tissue-specific transgenic and gene ablation approach demonstrate for the 102 first time that RNF40 exerts a profound tumor supportive function in the biology of HER2-driven mammary 103 carcinoma. In support of these in vivo findings, we show that RNF40 silencing leads to decreased cell 104 proliferation and specific transcriptional and epigenetic changes in HER2-positive human BC cells lines. Finally, 105 we unveil a previously undescribed role of RNF40-mediated H2B monoubiquitination in driving the expression of 106 specific genes regulating actin cytoskeleton dynamics (in vitro and in vivo) and the activity of the downstream 107 FAK-driven signaling cascade.

108

109 **RESULTS**

110 RNF40 is highly expressed in HER2-positive BC

111 While we and others have uncovered potential differing tumor-supportive or tumor-suppressive roles of 112 H2Bub1 and its E3 ligases RNF20 and RNF40 in ER-positive and triple negative BC (11,12,16), the role of this 113 epigenetic pathway in HER2-positive BC is currently unclear. Therefore, we investigated RNF40 expression and H2Bub1 levels by immunohistochemical staining of 176 primary BC tumors and 78 brain metastases. 114 115 Interestingly, examination of RNF40 and H2Bub1 staining revealed that all analyzed HER2-positive BC samples were positive for both markers (Fig.1A-C and Fig S1A). Moreover, HER2-positive metastatic BC samples showed a 116 117 particularly high expression of RNF40 compared to primary tumors (Fig.1A-C and Fig S1A). We next examined 118 the relationship between RNF40 mRNA levels and survival in HER2-positive BC patients using publically available 119 data and observed that high levels of RNF40 expression were associated with a reduced overall and relapse-free 120 survival (Fig.S1C and Fig.1D). Strikingly, in the same dataset, RNF40 mRNA expression was found to be 121 significantly higher in HER2-positive breast cancer tissues compared to normal mammary tissues (Fig.S1B). In 122 summary, these data suggest a potentially unexpected tumor supportive role of RNF40 in HER2-positive BC.

123 RNF40 plays a tumor supportive function in *Erbb2*-driven mammary carcinoma *in vivo*

124 Since RNF40 expression and activity were largely maintained in human HER2-positive BC, we hypothesized that a 125 loss of RNF40 may impair HER2-driven tumorigenesis in a mouse model system. Therefore, to test this 126 hypothesis, we utilized the MMTV-Erbb2 genetic mouse model initiating HER2-positive mammary lesions upon 127 overexpression of the Erbb2 proto-oncogene (coding for HER2) specifically in mammary epithelial cells (32). We generated a tri-transgenic MMTV-Erbb2; MMTV-Cre; Rnf40^{flox} mouse line with mammary tissue-specific co-128 129 expression of HER2 and Cre-recombinase, and a floxed Rnf40 allele. This approach enabled us to achieve a 130 simultaneous HER2 overexpression and mammary epithelium-specific ablation of Rnf40 (18,22). Consistent with our findings in human HER2-positive BC lesions, MMTV-Erbb2; Rnf40^{wt/wt} tumors did not display a loss of either 131 132 RNF40 or H2Bub1 (Fig. 1H) when compared to the adjacent normal mammary epithelium (Fig. S1F). Moreover, 133 immunohistochemical analyses confirmed that HER2 expression was unaffected by *Rnf40* deletion (Fig.1H). However, both heterozygous (Rnf40^{wt/fl}), and especially homozygous loss of Rnf40 (Rnf40^{fl/fl}) resulted in 134 135 dramatically increased tumor-free survival of MMTV-Erbb2 animals (Fig.1E). Remarkably, despite the high tumor

incidence in this mouse model (100% of Rnf40^{wt/wt} mice developed tumors after 220 days), 2 out of 14 Rnf40^{fl/fl} 136 137 animals (14%) never developed tumors even after 18 months observation (Fig.1E). Analyses of the tumor burden revealed that *Rnf40^{fl/fl}* mice developed significantly fewer tumors than *Rnf40^{wt/wt}* (Fig.1F) and loss of *Rnf40* led to 138 strongly reduced tumor growth kinetics (Fig.1G). Notably, Rnf40 loss did not induce morphological changes, as 139 visible in H&E staining of the Rnf40^{wt/wt} and Rnf40^{fl/fl} tumors (Fig.S1D). To estimate the efficiency of Rnf40 140 deletion in this model, we performed RNF40 immunohistochemical staining in *Rnf40^{wt/wt}* and *Rnf40^{fl/fl}* tumors. 141 Consistent with the lack of a complete block in tumor incidence and growth, Rnf40^{fl/fl} lesions displayed a 142 143 heterogeneous pattern of RNF40 expression (Fig.1H), suggesting that the few tumors that did develop in this 144 model were largely caused by an incomplete loss of the Rnf40 allele. This is further supported by the observation that both H2Bub1, as well the proliferation marker Ki67, displayed a similar heterogeneous 145 146 expression pattern as RNF40 (Fig.1H-I and Fig.S1E). Similar effects have been reported in a number of other 147 tumor types and with various Cre models, where occasional tumors did appear, which all retained some 148 expression of the floxed essential tumor driver gene of interest (33,34). Thus, we posit that these findings provide further support for the essential role of RNF40 in HER2-driven tumorigenesis to the extent that rare, 149 150 RNF40/H2Bub1-expressing "escaper" cells are positively selected for during tumorigenesis and tumor 151 progression. Taken together, these results demonstrate that RNF40 plays an essential supportive function in 152 HER2-driven mammary tumor initiation and progression.

153 RNF40 loss impairs oncogenic properties of HER2-positive BC cells in vitro

We next sought to investigate the underlying molecular mechanisms determining the dependence of HER2 positive BC on RNF40. In order to achieve this goal, we selected two different human HER2-positive BC cell lines (HCC1954, SKBR3) and assessed different parameters related to their tumorigenic properties following siRNAmediated RNF40 knockdown. RNF40 depletion and concomitant loss of H2Bub1 in both cell lines (Fig.2A, Fig.S2A-B) resulted in reduced cellular proliferation compared to control transfected cells (Fig.2B-C; Fig.S2A-B). Furthermore, growth kinetics (Fig.2C and Video in supplements), clonogenic capacity (Fig.2D) and tumor sphere formation (Fig.2E) were strongly impaired upon RNF40 loss in both cell lines. In support of these results, an 161 analysis of the data in the DepMap portal (https://depmap.org/), which contains information for gene essentiality deriving from various RNAi and CRISPR screens, revealed that HER2-positive breast cancer cell lines 162 163 are significantly impacted by RNF40 loss by CRISPR/Cas9-mediated deletion, further confirming a particularly 164 important role for RNF40 in this subtype of breast cancer (Fig.S2C). Consistently, the levels of the proliferation 165 marker Ki67 were strongly reduced in both HER2-positive BC cell lines upon RNF40 depletion (Fig.2F). Finally, we also tested the migration potential of HCC1954 cells upon RNF40 depletion in trans-well migration (Fig.2G) and 166 167 gap closure assays (Fig.S2D). Notably, both approaches showed impaired cellular motility upon loss of RNF40. Together these findings support our in vivo findings that RNF40 expression is essential for maintaining 168 169 tumorigenic properties of HER2-positive BC cells both in vitro and in vivo.

170 RNF40 regulates actin cytoskeleton-related genes in HER2-positive BC cells

171 Based on the dramatic effects observed on HER2-driven tumorigenesis in vivo and in vitro, we tested whether 172 the activity of the signaling cascade downstream of HER2 may be directly affected by RNF40 loss. However, 173 while the HER2 inhibitor Lapatinib (lap) significantly blocked ERK and AKT phosphorylation in the HER2-positive 174 HCC1954 cell line, both pathways remained intact following RNF40 depletion (Fig.3A). Therefore, given the 175 direct epigenetic role of H2Bub1 in facilitating gene transcription, we performed mRNA-sequencing analyses of 176 HCC1954 cells following RNF40 depletion or control siRNA-transfection and identified 360 up- and 324 down-177 regulated genes (|log2 fold change|>0.6; p-val<0.05) (Fig.3B). Consistent with our previous findings in colorectal 178 cancer (19), Gene Set Enrichment Analysis (GSEA) identified a significant enrichment for a gene signature 179 associated with hallmarks of apoptosis, potentially explaining the reduced oncogenic properties (Fig.3C and 180 S3B). Increased apoptosis could be confirmed by microscopic time lapse analyses (see videos in supplements), 181 higher levels of cleaved caspase 3 and cleaved PARP in Western blot (Fig.3D) and an increase in Annexin V-182 positive cells in FACS-based analyses in HCC1954 cells (Fig.3E). Given the fact that RNF40 depletion not only resulted in decreased cell number, but also dramatically affected cell migration, we performed additional gene 183 184 ontology analyses using the EnrichR tool (https://amp.pharm.mssm.edu/Enrichr/) and identified an enrichment 185 of genes associated with the actin cytoskeleton regulatory pathway as being downregulated following RNF40 186 depletion (Fig.3F and S3C). We selected genes from this set and confirmed the downregulation of Vav Guanine

187 Nucleotide Exchange Factor 3 (*VAV3*), Rho Associated Coiled-Coil Containing Protein Kinase 1 (*ROCK1*), LIM 188 Domain Kinase 2 (*LIMK2*) and Profilin 2 (*PFN2*), which directly control filamentous actin dynamics, both at the 189 mRNA (Fig.3G and Fig.S3A) and protein (ROCK1, VAV3; Fig.3H) levels.

190 Phosphorylation of the cofilin protein by LIMK downstream of ROCK1 plays an important role in controlling actin 191 cytoskeleton dynamics (35). In its active unphosphorylated form, cofilin destabilizes F-actin and leads to actin 192 depolymerization. We therefore assessed cofilin phosphorylation (p-cofilin) via western blotting and observed 193 strongly reduced levels in RNF40-depleted HCC1954 cells (Fig.4A). Consistently, phalloidin staining further 194 confirmed the impairment of F-actin formation upon RNF40 depletion in HCC1954 (Fig.4C) and SKBR3 cells 195 (Fig.S4A) and these effects could be phenocopied by inhibition of ROCK1 by RKI-1447 (Fig.4A and C) or siRNAmediated knockdown of VAV3 (Fig.4B). Importantly, these effects could also be confirmed in vivo where cofilin 196 phosphorylation was also significantly decreased in Rnf40^{fl/fl} tumors compared to wild type Rnf40 tumors 197 198 (Fig.4D). Together, these data confirm the *in vitro* and *in vivo* importance of RNF40 in controlling actin 199 cytoskeletal dynamics in HER2-positive BC.

200 In addition to the established role of the ROCK1 pathway in controlling actin cytoskeletal dynamics, this pathway 201 also plays a central role in suppressing apoptosis and potentiating cell survival (36–39). Notably, the potent 202 ROCK inhibitor RKI-1447 was shown to elicit a pronounced anti-tumorigenic effect on the same Erbb2-driven 203 mammary carcinoma mouse model used in our current study (37). Thus, we hypothesized that the dysregulation 204 of the ROCK1-depedent actin regulatory pathway may play a central role in the apoptotic phenotype induced by 205 RNF40 loss. Indeed, RKI-1447 treatment led to impaired HCC1954 cell proliferation (Fig.S4B) and the induction of 206 caspase 3 cleavage (Fig.4E). We therefore conclude that RNF40 has a decisive impact on the apoptotic rate of 207 HER2-positive BC cells by regulating important members of the VAV3-ROCK1-LIMK2-PFN2 axis.

Focal adhesion complexes are cell-to-substrate adhesion structures that are tightly coupled to F-actin dynamics and significantly contribute to preserving anti-apoptotic pathways via the Focal Adhesion Kinase (FAK) (38,40). Since we demonstrated a crucial function of RNF40 in regulating the formation of F-actin stress fibers, we hypothesized that RNF40 depletion may influence the cell growth potential of HER2-positive BC cells by

impairing focal adhesion signaling via impaired actin dynamics. To test this hypothesis, we first estimated the median area of focal adhesions via immunofluorescent staining for vinculin, one of the molecules which bridges focal adhesion complexes and F-actin. Indeed, the area of focal adhesion was substantially decreased upon RNF40 depletion and these effects could be phenocopied by VAV3 depletion (Fig.4G). Furthermore, the levels of active phosphorylated FAK (p-FAK) were decreased upon RNF40 depletion in HCC1954 cells and could be phenocopied by ROCK inhibition (Fig.4F). Moreover, consistent with these findings, direct inhibition of FAK led to a significant decrease in HCC1954 cell number (Fig. S4D).

219 To ensure the causality of the impaired tumorigenic phenotype of RNF40-silenced HCC1954 cells due to an 220 impaired actin regulatory pathway, we examined the effects of restoring this signaling cascade. For this purpose, 221 we treated HCC1954 cells with an allosteric sphingosine 1-phosphate receptor-3 agonist (CYM-5441), which was 222 shown to activate actin polymerization as well as increase cancer stem cell expansion in BC (41,42). Treatment 223 of RNF40-depleted HCC1954 cells with CYM-5441 significantly rescued apoptosis as measured by Annexin V 224 staining (Fig.41) and caspase 3/7 activity (Fig.S4C). Additionally, treatment with either CYM-5441 (Fig.4J) or 225 lysophosphatidic acid (Fig.S4E), which has also been shown to activate this pathway (43), partially rescued the 226 impaired proliferation of HCC1954 cells following RNF40 depletion. Notably, this rescue was prevented by 227 treatment with RKI-1447 (Fig.S4F-G), confirming that partial restoration of the actin regulatory pathway is 228 central to the observed rescuing effects. Collectively, these findings establish RNF40 as an important regulator of 229 HER2-positive BC cell viability by regulating the actin regulatory process in vitro and in vivo via the regulation of 230 the VAV3-ROCK1-LIMK2-PFN2 and focal adhesion signaling cascade.

231

232 RNF40 regulates the VAV3-ROCK-LIMK2-PFN2 axis through H2Bub1-H3K4me3 trans-histone crosstalk

Previous studies from other groups demonstrated a crosstalk between H2Bub1 and H3K4 tri-methylation (H3K4me3) both in yeast and human systems (26,29,30). Moreover, we recently demonstrated that RNF40mediated H2B monoubiquitination specifically governs the transcriptional start site- (TSS-) proximal broadening of H3K4me3 into the transcribed region to facilitate transcriptional elongation of a number of moderately

237 H2Bub1-marked genes in mouse embryo fibroblasts (MEFs) (22). To examine if RNF40 controls the expression of genes of the actin regulatory network by modulating H2Bub1 and H3K4me3 levels, we performed chromatin 238 239 immunoprecipitation sequencing (ChIP-seq) analyses for H2Bub1 and H3K4me3 in HCC1954 cells (Fig.S5A). 240 Strikingly, consistent with our previous findings (22), RNF40-dependent genes showed lower levels of H2Bub1 241 occupancy compared to unregulated genes or genes up-regulated following RNF40 depletion (Fig.5A). Given our 242 previous finding that H3K4me3 "peak narrowing" is a distinct epigenetic feature involved in the regulation of 243 RNF40-dependent genes, we identified peaks displaying either an increase or a global or partial (3' narrowing) 244 decrease of H3K4me3 occupancy upon RNF40 silencing in HCC1954 cells (Fig.5B). We then utilized the identified 245 regions for differential binding (Diffbind) analyses and observed that the majority of the regions influenced by 246 RNF40 depletion markedly lost H3K4me3 (8,518 regions), whereas only a few regions gained H3K4me3 247 occupancy (351 regions) (Fig.5C and Fig.5D). Interestingly, most of the regions showing decreased H3K4me3 248 (Fig.5C) were located proximal to TSS regions (Fig.S5B). Moreover, regions displaying no changes in H3K4me3 249 occupancy show only a mild peak narrowing, while regions displaying a significant loss of H3K4me3 occupancy 250 exhibit a stronger peak narrowing upon RNF40 depletion (Fig.5D and S5C). Importantly, consistent with our gene expression analyses, TSS-associated regions displaying decreased H3K4me3 occupancy following RNF40 251 252 depletion included genes associated with the actin regulatory pathway signature (Fig.S5D).

253 To further investigate the behavior of H3K4me3 occupancy at the TSS of regulated genes, we plotted H3K4me3 254 occupancy on robustly down-, up- and unregulated genes under control or RNF40-depleted conditions. 255 Consistent with our analyses based on changes in H3K4me3 occupancy, genes downregulated upon RNF40 256 silencing displayed the most prominent decrease in H3K4me3 in the gene body (the 3' end of the peak) 257 compared to unregulated or upregulated genes (Fig.5E-F). Importantly, a significant fraction of downregulated 258 genes (162 out of 324) showed a concomitant decrease in H3K4me3 near the TSS ("Group A" in Fig. 5G). 259 Moreover, Group A was enriched for genes involved in the actin dynamics regulatory pathway. The decrease in 260 H3K4me3 spreading into the body of the ROCK1, LIMK2 and VAV3 genes could be validated by ChIP-qPCR 261 (Fig.S5E). As a control, we identified a group of genes with a similar size and similar expression range as the

262 Group A (Group C), whose expression was not affected by RNF40 knockdown, but was characterized by a milder 263 reduction of H3K4me3 occupancy (Fig.5G and Fig.5H). Under normal culture conditions, genes of Group A 264 harbored lower H2Bub1 levels than the genes of Group C, but comparable H3K4me3 levels and peak height 265 (Fig.5J and Fig.S5F-G). Interestingly, Group A genes presented a more profound H3K4me3 peak narrowing upon 266 RNF40 depletion compared to the control group. The 162 genes found to be downregulated at the mRNA level 267 but not showing any H3K4me3 loss (Group B) showed overall lower expression values and displayed only 268 negligible levels of H2Bub1 across their gene body (Fig.5H-J and Fig.S5G). We therefore concluded that the 269 genes within Group B may likely be indirect downstream targets of RNF40-mediated H2B monoubiguitination. 270 Together, these findings support the hypothesis that the actin regulatory gene network is dependent on direct 271 epigenetic regulation by RNF40 through modulation of H2Bub1 and a trans-histone cross-talk with H3K4me3 272 levels in HER2-positive BC cells.

273 To further characterize the epigenetic differences distinguishing Group A and C, and which may help to explain 274 the RNF40-dependency of Group A genes, we analyzed ChIP-seq data for several other histone modifications in 275 HCC1954 cells (44,45). These analyses revealed that the occupancy of the active histone marks H3K27ac and 276 H3K9ac was slightly higher at the TSS of Group C genes in comparison to Group A, while the elongation-277 associated modifications, H3K36me3 and H3K79me2, were dramatically higher in the gene body of Group C. 278 Accordingly, RNA Polymerase II (RNApol II) occupancy was also higher on genes in Group C compared to the 279 other groups (Fig.5J). Together, when compared to the genes within Groups A and B, genes within Group C 280 display a more pronounced occupancy of epigenetic marks associated with active gene transcription (46). Thus, 281 these additional epigenetic modifications may help to compensate for the loss of H2Bub1 following RNF40 depletion, whereas lower levels of these active marks on Group A genes may render these to be more sensitive 282 283 to changes in H2Bub1 occupancy.

In summary, we conclude that RNF40 is a major epigenetic regulator of the actin regulatory gene network in HER2-positive BC cells via H2B monoubiquitination and the downstream trans-histone control of H3K4me3 occupancy in the transcribed region.

287

288 Discussion

289 H2B monoubiguitination has previously been reported to serve a tumor suppressive function with its levels 290 gradually decreasing during cancer progression. Interestingly, the role of RNF20, a subunit of the obligate 291 heterodimeric RNF20/RNF40 E3 ubiquitin ligase complex catalyzing the deposition of H2Bub1, is more 292 contradictory and seems to exert opposing functions depending on cancer type or subtype (16,17). To date, only 293 few studies focused on RNF40 expression in cancer. Upon examination of a cohort of both primary BC and brain 294 metastases, we identified the loss of RNF40 expression and H2Bub1 as rare events in primary and metastatic 295 HER2-positive lesions. Publically available datasets corroborate our results, showing only a very low rate of 296 genetic alterations (<1%) causing loss of RNF40 function in BC (cbioportal.org, data not shown). Interestingly, the same datasets report a much higher frequency of RNF40 locus amplification in malignancies of the breast (4-297 298 6%) accompanied by increased RNF40 expression levels in tumors compared to normal tissues (TCGA dataset). 299 Additionally, high expression levels of RNF40 were associated with an unfavorable outcome in HER2-positive BC 300 patients. Finally, the genetic model for RNF40 loss in endogenous HER2-driven mammary carcinomas used in 301 this study supported the human patient data, arguing for a tumor-supporting role for RNF40 in HER2-dependent 302 BC. Together, our data do not support a general tumor suppressive function of RNF40 and H2Bub1.

303 Upon investigating the transcriptional and molecular epigenetic mechanisms rendering HER2-positive BC cells 304 critically dependent upon RNF40, we observed that loss of RNF40 had a profound impact on the deposition of 305 the H3K4me3 histone mark leading to a significant "peak narrowing" in the transcribed region downstream of 306 the TSS on regulated genes. The crosstalk between H2Bub1 and H3K4me3 has been intensively studied in the 307 past and has been attributed to the trans-regulation of the histone methyl transferase activity of the COMPASS 308 family of H3K4 methyltransferases by H2Bub1 (8,22,47). Our previous work revealed that RNF40 promotes the 309 expression of a specific subset of genes displaying a high elongation rate via modulation of H3K4me3 peak 310 broadening in a context-specific manner (22). Consistently, our new integrated datasets in HER2-positive BC not only further confirm that RNF40-dependent genes display a more profound tendency of H3K4me3 domain 311

narrowing upon RNF40 depletion, but also show that these genes display a less pronounced accumulation of various activating epigenetic marks compared to RNF40-independent genes. Interestingly, RNF40-dependent genes also displayed lower H3K79me2 levels, another histone mark that was shown to function downstream of H2Bub1 to epigenetically regulate gene expression, implying that an additional epigenetic layer helps to control the transcriptional output of RNF40/H2Bub1-independent genes (28). We therefore hypothesized that this specific group of genes is rendered particularly sensitive to H2Bub1 loss upon RNF40 depletion due to their overall less active chromatin status.

319 Strikingly, a large fraction of the genes identified in this study as being RNF40-dependent are well known 320 effectors of the actin regulatory pathway. Next to the reported implication of RNF40 in DNA damage response 321 (48), replication stress (14), microtubule spindle organization (49), inflammation (18) and regulation of hormone 322 receptor activity (12,20), the discovery that the maintenance of actin dynamics critically depends upon RNF40 in 323 HER2-positive BC is both new and of significant interest. Notably, HER2-positive BC cells were previously shown 324 to heavily rely on intact actin dynamics for cancer cell viability, motility and metastasis (39,50). Importantly, we 325 specifically identified VAV3, ROCK1, LIMK2 and PFN2 as RNF40-dependent genes and confirmed the functional 326 consequence of their impaired expression, which resulted in decreased cofilin phosphorylation both in vitro and 327 in vivo, and decreased F-actin abundance and impaired actin dynamics. Importantly, we identified the ROCK1 328 kinase as a central RNF40-regulated factor controlling the actin regulatory pathway, as its inhibition via the 329 potent ROCK inhibitor RKI-1447 was able to phenocopy the impaired tumorigenic phenotype caused by RNF40 330 loss. Interestingly, activation of the actin cytoskeleton signaling pathway by treating RNF40-depleted cells with 331 an S1PR₃ agonist partially rescued these effects. Therefore, these data strongly suggest that the imbalance in the 332 control of actin dynamics in RNF40-depleted cells is largely a ROCK1-dependent phenomenon and support a 333 previous study displaying the anti-tumorigenic effect of RKI-1447 in HER2-driven BC in vivo (37).

In addition to the central role of actin cytoskeleton dynamics in controlling cellular migration, the ROCK and focal adhesion kinase signaling pathway also has a critical function in suppressing apoptosis (37,51). While we previously identified a role for RNF40 in suppressing apoptosis in colorectal cancer cells via expression of anti-

apoptotic members of the BCL2 family of proteins (19), our current results suggest that RNF40 suppresses 337 338 programmed cell death in HER2-positive BC in a distinct manner via maintenance of ROCK-dependent focal 339 adhesion kinase signaling. Indeed, focal adhesion structures decreased in size with a concomitant decrease in FAK kinase activity upon either RNF40 depletion or ROCK1 inhibition. Our data suggest that RNF20/RNF40-driven 340 341 H2B monoubiguitination plays a decisive, context-specific function in HER2-positive BC by controlling the actin 342 regulatory circuit and the downstream focal adhesion kinase-driven signaling cascade to maintain both anti-343 apoptotic signaling and control cellular migration in cancer cells. It is therefore attractive to speculate that a 344 simultaneous inhibition of the RNF20/RNF40 E3 ubiquitin ligase activity together with inhibition of either ROCK1 345 or FAK might provide synergistic effects in the treatment of HER2-positive BC.

Together, our data support a context-dependent role of RNF40 and H2B monoubiquitination in breast carcinogenesis and suggest that the RNF20/RNF40 E3 ubiquitin ligase and/or its upstream regulators or downstream targets may serve as attractive targets for the development of new anti-cancer strategies in HER2positive BC.

351 Acknowledgments

We would like to thank S. Bolte, N. Molitor and the staff of the European Neuroscience Institute Göttingen for assistance in the animal handling administration, F. Alves (Translational Molecular Imaging, Max Planck Institute for Experimental Medicine, Göttingen) for access to the IncuCyte[®] Live Cell Analysis System (Sartorius AG), S. Lutz (Institute of Pharmacology and Toxicology, University Medical Center Göttingen, Göttingen) for providing the vinculin antibody and M. Dobbelstein for reagents for measuring caspase 3/7 activity (Department of Molecular Oncology, Göttingen).

358

359 Materials and Methods

360 Animal handling and mouse model generation

Animals were housed under specific pathogen-free (SPF) conditions and in accordance with the animal rights laws and regulations of Lower-Saxony (LAVES, registration number #15/1754). For more details, please refer to the Supplementary Data.

364 Histology of human and murine tissues and publically available dataset analyses

Tissue microarrays of human primary and metastatic breast cancer were generated at the University Medical Center Hamburg Eppendorf Germany (local ethical committee approval number: OB/V/03 and MC-267/13, respectively) in accordance with the ethical standards of the 1964 Declaration of Helsinki. RNF40 and H2Bub1 scoring was established based on the staining intensity (null=no detectable staining, low=weak staining intensity, high=strong staining intensity). Detailed staining procedures, antibodies used for immunohistochemical staining are provided in the Supplementary Data.

371 Publically available datasets

The Kaplan-Meier plotter (kmplot.com) and The Cancer Genome Atlas (TCGA)-derived publically available datasets were used to examine the association of *RNF40* expression with Relapse-Free Survival (RFS) or Overall Survival (OS) of HER2-positive BC patients. Please refer to the Supplementary Data for BC subtype classification

parameters. Publically available datasets for histone modifications of active transcription in HCC1954 cells
(GSE85158 and GSE72956) were downloaded from Gene Expression Omnibus (www.ncbi.nlm.nih.gov/geo/)
(44,45).

378 *Cell culture, transfections and functional assays*

HCC1954 (ATCC[®] CRL-2338[™]) and SKBR3 (ATCC[®] HTB-30[™]) cells were purchased from the American Type
Culture Collection (ATCC). siRNA transfections were performed using Lipofectamine[®] RNAiMAX (Invitrogen)
according to the manufacturer's guidelines. Proliferation kinetics as well tumor spheres were recorded using
Celigo[®] S imaging cytometer (Nexcelom Bioscience LLC) and IncuCyte[®] Live Cell Analysis System (Sartorius AG).
Colonies and migrated cells from trans-well assay were washed with PBS, fixed, stained and scanned with an
Epson Perfection V700 Photo. Detailed protocols for siRNA transfection of both cell lines are available in the
Supplementary Data.

386 Immunofluorescence microscopy

Cells were plated and transfected on coverslips and grown for another 72 h. Cells were then washed with PBS, cross-linked with 4% paraformaldehyde and permeabilized with 1% Triton X-100 in PBS or TBS for 10 min, blocked for 1 h and incubated with the primary antibody overnight. Coverslips were washed and secondary antibody was applied with DAPI and eventually Alexa555-phalloidin for 1 hour at room temperature. Coverslips were washed and mounted on microscope slides. A detailed protocol as well for a list of antibodies is available in the Supplementary Data.

393 Microscopy

Immunohistochemistry (IHC) pictures were taken with a Zeiss Axio Scope A1. Bright-field images of cultured cells were taken with a Nikon Eclipse S100 inverted microscope and immunofluorescence pictures with a Zeiss LSM 510 Meta confocal microscope. Fluorescence intensity was quantified using the ImageJ software. Image analysis workflow is described in the Supplementary Data.

398

400

401 Annexin and caspase 3/7 activity assay

For annexin V staining, cells were tryprinized and resuspended in binding buffer at 72 hours post-transfection
and incubated with Annexin V-FITC (Southern Biotech) and propidium iodide (Sigma Aldrich) for 15 min at room
temperature. Samples were analyzed using a Guava EasyCyte Plus flow cytometer (Guava Technologies).
The kinetic apoptosis assay using caspase 3/7 was performed according to the manufacturer's instructions (CS1V0002(3)-1, ViaStainTM Live Caspase 3/7 Detection Kit, Nexcelom). Scanning was performed at time points 24,

- 407 48 and 72 hours post transfection using a Celigo[®] S imaging cytometer (Nexcelom Bioscience LLC). For detailed
- 408 protocols, please refer to the Supplementary Data.

409 ChIP library preparation and data analysis

410 Chromatin immunoprecipitation was performed as described previously (52) 72 hours after transfection with 411 control or RNF40 siRNAs using antibodies against H2Bub1 (Cat. No. 5546S, Cell Signaling Technology) and 412 H3K4me3 (Cat. No. C15410003-50, Diagenode). Next generation sequencing libraries were prepared using the 413 Microplex Library Preparation kit v2 (Diagenode, Cat.No. C05010011) according to manufacturer's instructions 414 and samples were sequenced (single-end 50 bp) on a HiSeq4000 (Illumina) at the Transcriptome and Genome 415 Analysis Laboratory (TAL) at the University Medical Center Göttingen. Processing of sequencing data was 416 performed in the Galaxy environment provided by the "Gesellschaft für wissenschaftliche Datenverarbeitung 417 mbH Göttingen" (galaxy.gwdg.de). Briefly, ChIP-seq reads were mapped to the hg19 reference genome assembly 418 using Bowtie2 (version 2.3.2.2). PCR duplicates were removed using the RmDup tool (version 2.0.1). The 419 deeptools suite (version 3.2.0.0.1) was utilized to generate normalized coverage files (bamCoverage), call peak 420 changes (bigwigCompare), and to generate aggregate plots and heatmaps (computeMatrix and plotHeatmap). 421 Occupancy profiles were visualized using the Integrative Genomics Viewer (IGV 2.4.8). Detailed analysis 422 workflow is available in Supplementary Data.

423 RNA library preparation and data analysis

RNA sequencing libraries were generated from HCC1954 cells at 72 hours post-transfection with the NEXTFLEX[®] Rapid Directional RNA-Seq Kit (Bioo Scientific, Catalog #NOVA-5138-07) according to the manufacturer's instructions and samples were sequenced (single-end 50 bp) on a HiSeq4000 (Illumina) at the TAL. RNA-seq data were processed in the Galaxy environment. Raw reads were trimmed (FASTQ Trimmer), mapped to the reference genome hg19 using TopHat (version 2.1.1) and read counts per gene was calculated with featureCounts. Finally, differential gene expression analysis and normalized counts were obtained using DESeq2.

430 Detailed analysis workflow is available in Supplementary Data.

431 References

432	1.	Bray F, Ferlay J, Soerjomataram I, Siegel RL, Torre LA, Jemal A. Global cancer statistics 2018: GLOBOCAN
433		estimates of incidence and mortality worldwide for 36 cancers in 185 countries. CA Cancer J Clin.
434		2018;68:394–424.
435	2.	Coleman MP, Quaresma M, Berrino F, Lutz J-MM, De Angelis R, Capocaccia R, et al. Cancer survival in five
436		continents: a worldwide population-based study (CONCORD). Lancet Oncol. 2008;9:730–56.
437	3.	Perou CM, Sørlie T, Eisen MB, van de Rijn M, Jeffrey SS, Rees C a, et al. Molecular portraits of human
438		breast tumours. Nature. 2000;406:747–52.
439	4.	Nahta R, Yu D, Hung M-C, Hortobagyi GN, Esteva FJ. Mechanisms of Disease: understanding resistance to
440		HER2-targeted therapy in human breast cancer. Nat Clin Pract Oncol. 2006;3:269–80.
441	5.	Hanahan D, Weinberg RAA. Hallmarks of Cancer: The Next Generation. Cell. 2011;144:646–74.
442	6.	Huang Y, Nayak S, Jankowitz R, Davidson NE, Oesterreich S. Epigenetics in breast cancer: what's new?
443		Breast Cancer Res. 2011;13:225.
444	7.	Mohammad HP, Barbash O, Creasy CL. Targeting epigenetic modifications in cancer therapy: erasing the
445		roadmap to cancer. Nat Med. 2019;25:403–18.
446	8.	Karpiuk O, Najafova Z, Kramer F, Hennion M, Galonska C, Konig A, et al. The Histone H2B
447		Monoubiquitination Regulatory Pathway Is Required for Differentiation of Multipotent Stem Cells. Mol
448		Cell. 2012;46:705–13.
449	9.	Fuchs G, Shema E, Vesterman R, Kotler E, Wolchinsky Z, Wilder S, et al. RNF20 and USP44 regulate stem
450		cell differentiation by modulating H2B monoubiquitylation. Mol Cell. 2012;46:662–73.
451	10.	Chen S, Li J, Wang D-LL, Sun F-LL. Histone H2B lysine 120 monoubiquitination is required for embryonic

452 stem cell differentiation. Cell Res. 2012;22:1402–5.

- 453 11. Bedi U, Scheel AH, Hennion M, Begus-Nahrmann Y, Rüschoff J, Johnsen SA. SUPT6H controls estrogen
- receptor activity and cellular differentiation by multiple epigenomic mechanisms. Oncogene. 454

455 2015;34:465-73.

- 456 12. Prenzel T, Begus-Nahrmann Y, Kramer F, Hennion M, Hsu C, Gorsler T, et al. Estrogen-dependent gene
- transcription in human breast cancer cells relies upon proteasome-dependent monoubiguitination of 457
- 458 histone H2B. Cancer Res. 2011;71:5739-53.
- 459 Zhang K. Wang J. Tong TR. Wu X. Nelson R. Yuan Y-CC, et al. Loss of H2B monoubiguitination is associated 13. 460 with poor-differentiation and enhanced malignancy of lung adenocarcinoma. Int J Cancer. 2017;141:766-77.
- 461
- 462 Chernikova SB, Razorenova O V., Higgins JP, Sishc BJ, Nicolau M, Dorth JA, et al. Deficiency in mammalian 14. histone H2B ubiquitin ligase Bre1 (Rnf20/Rnf40) leads to replication stress and chromosomal instability. 463 464 Cancer Res. 2012;72:2111–9.
- 465 15. Tarcic O, Granit RZ, Pateras IS, Masury H, Maly B, Zwang Y, et al. RNF20 Links Histone H2B Ubiguitylation 466 with Inflammation and Inflammation-Associated Cancer. Cell Rep. 2016;24:694–704.
- 467 16. Tarcic O, Granit RZ, Pateras IS, Masury H, Maly B, Zwang Y, et al. RNF20 and histone H2B ubiquitylation exert opposing effects in Basal-Like versus luminal breast cancer. Cell Death Differ. 2017;24:694–704. 468
- 469 17. Johnsen SA. The enigmatic role of H2Bub1 in cancer. FEBS Lett. Federation of European Biochemical 470 Societies; 2012;586:1592-601.
- 471 18. Kosinsky RL, Chua RL, Qui M, Saul D, Mehlich D, Ströbel P, et al. Loss of RNF40 decreases NF-κB activity in 472 colorectal cancer cells and reduces colitis burden in mice. J Crohn's Colitis. Oxford University Press; 2019;13:362-73. 473
- 474 19. Schneider D, Chua RL, Molitor N, Feda H, Maria RE, Prokakis E, et al. The E3 ubiguitin ligase RNF40
- 475 suppresses apoptosis in colorectal cancer cells. Clin Epigenetics. 2019;11:98.

- 476 20. Jaaskelainen T, Makkonen H, Visakorpi T, Kim J, Roeder RG, Palvimo JJ, et al. Histone H2B ubiquitin ligases
- 477 RNF20 and RNF40 in androgen signaling and prostate cancer cell growth. Mol Cell Endocrinol.
- 478 2012;350:87–98.

481

22.

479 21. Minsky N, Shema E, Field Y, Schuster M, Segal E, Oren M. Monoubiquitinated H2B is associated with the
480 transcribed region of highly expressed genes in human cells. Nat Cell Biol. 2008;10:483–8.

Xie W, Nagarajan S, Baumgart SJ, Kosinsky RL, Najafova Z, Kari V, et al. RNF40 regulates gene expression

- 482 in an epigenetic context-dependent manner. Genome Biol. 2017;18:32.
- 483 23. Fuchs G, Hollander D, Voichek Y, Ast G, Oren M. Cotranscriptional histone H2B monoubiguitylation is
- 484 tightly coupled with RNA polymerase II elongation rate. Genome Res. 2014;24:1572–83.
- 485 24. Pirngruber J, Shchebet A, Schreiber L, Shema E, Minsky N, Chapman RD, et al. CDK9 directs H2B
- 486 monoubiquitination and controls replication-dependent histone mRNA 3'-end processing. EMBO Rep.
 487 2009;10:894–900.
- 488 25. Pavri R, Zhu B, Li G, Trojer P, Mandal S, Shilatifard A, et al. Histone H2B Monoubiquitination Functions
- 489 Cooperatively with FACT to Regulate Elongation by RNA Polymerase II. Cell. 2006;125:703–17.
- 490 26. Sun Z-WW, Allis CD. Ubiquitination of histone H2B regulates H3 methylation and gene silencing in yeast.
 491 Nature. 2002;418:104–8.
- 492 27. Ng HH, Xu R-MM, Zhang Y, Struhl K. Ubiquitination of histone H2B by Rad6 is required for efficient Dot1493 mediated methylation of histone H3 lysine 79. J Biol Chem. 2002;277:34655–7.
- Valencia-Sánchez MI, De Ioannes P, Wang M, Vasilyev N, Chen R, Nudler E, et al. Structural Basis of Dot1L
 Stimulation by Histone H2B Lysine 120 Ubiquitination. Mol Cell. 2019;74:1010-1019.e6.
- 496 29. Kim J, Guermah M, McGinty RK, Lee J-SS, Tang Z, Milne TA, et al. RAD6-Mediated Transcription-Coupled
- 497 H2B Ubiquitylation Directly Stimulates H3K4 Methylation in Human Cells. Cell. 2009;137:459–71.

- 498 30. Kim J, Hake SB, Roeder RG. The human homolog of yeast BRE1 functions as a transcriptional coactivator
- 499 through direct activator interactions. Mol Cell. 2005;20:759–70.
- 500 31. Chen K, Chen Z, Wu D, Zhang L, Lin X, Su J, et al. Broad H3K4me3 is associated with increased
- 501 transcription elongation and enhancer activity at tumor-suppressor genes. Nat Genet. 2015;47:1149–57.
- 502 32. Guy CT, Webster MA, Schaller M, Parsons TJ, Cardiff RD, Muller WJ. Expression of the neu protooncogene
- 503 in the mammary epithelium of transgenic mice induces metastatic disease. Proc Natl Acad Sci U S A.
- 504 1992;89:10578-82.
- Miao RY, Drabsch Y, Cross RS, Cheasley D, Carpinteri S, Pereira L, et al. MYB is essential for mammary
 tumorigenesis. Cancer Res. 2011;71:7029–37.
- 507 34. Costa TDF, Zhuang T, Lorent J, Turco E, Olofsson H, Masia-Balague M, et al. PAK4 suppresses RELB to
- 508 prevent senescence-like growth arrest in breast cancer. Nat Commun. Nature Publishing Group; 2019;10.
- 509 35. Maciver SK, Hussey PJ. The ADF/cofilin family: actin-remodeling proteins. Genome Biol.
- 510 2002;3:reviews3007.1.
- 511 36. Desouza M, Gunning PW, Stehn JR. The actin cytoskeleton as a sensor and mediator of apoptosis.
- 512 Bioarchitecture. 2012;2:75–87.
- 513 37. Patel RA, Forinash KD, Pireddu R, Sun Y, Sun N, Martin MP, et al. RKI-1447 is a potent inhibitor of the Rho-

associated ROCK kinases with anti-invasive and antitumor activities in breast cancer. Cancer Res.

- 515 2012;72:5025–34.
- S16 38. Chrzanowska-Wodnicka M, Burridge K. Rho-stimulated contractility drives the formation of stress fibers
 and focal adhesions. J Cell Biol. 1996;133:1403–15.
- 518 39. Tavares S, Vieira AF, Taubenberger AV, Araújo M, Martins NP, Brás-Pereira C, et al. Actin stress fiber
- 519 organization promotes cell stiffening and proliferation of pre-invasive breast cancer cells. Nat Commun.
- 520 2017;8:15237.

- 521 40. Choong G, Liu Y, Templeton DM. Cadmium affects focal adhesion kinase (FAK) in mesangial cells:
- 522 involvement of CaMK-II and the actin cytoskeleton. J Cell Biochem. 2013;114:1832–42.
- 41. Donati C, Bruni P. Sphingosine 1-phosphate regulates cytoskeleton dynamics: implications in its biological
 response. Biochim Biophys Acta. 2006;1758:2037–48.
- 525 42. Wang Y-C, Tsai C-F, Chuang H-L, Chang Y-C, Chen H-S, Lee J-N, et al. Benzyl butyl phthalate promotes
- 526 breast cancer stem cell expansion via SPHK1/S1P/S1PR3 signaling. Oncotarget. 2016;7:29563–76.
- 43. Yung YC, Stoddard NC, Chun J. LPA receptor signaling: pharmacology, physiology, and pathophysiology. J
 528 Lipid Res. 2014;55:1192–214.
- 529 44. Franco HL, Nagari A, Malladi VS, Li WW, Xi Y, Richardson D, et al. Enhancer transcription reveals subtype-

530 specific gene expression programs controlling breast cancer pathogenesis. Genome Res. 2018;28:159–70.

- 45. Malladi S, Macalinao DG, Jin X, He L, Basnet H, Zou Y, et al. Metastatic Latency and Immune Evasion
 through Autocrine Inhibition of WNT. Cell. 2016;165:45–60.
- 533 46. Zhang T, Cooper S, Brockdorff N. The interplay of histone modifications writers that read. EMBO Rep.
 534 EMBO; 2015;16:1467–81.
- 535 47. Pirngruber J, Shchebet A, Johnsen SA. Insights into the function of the human P-TEFb component CDK9 in

the regulation of chromatin modifications and co-transcriptional mRNA processing. Cell Cycle.

537 2009;8:3636–42.

- Kari V, Shchebet A, Neumann H, Johnsen SA. The H2B ubiquitin ligase RNF40 cooperates with SUPT16H to
 induce dynamic changes in chromatin structure during DNA double-strand break repair. Cell Cycle. Taylor
 and Francis Inc.; 2011;10:3495–504.
- 541 49. Duan Y, Huo D, Gao J, Wu H, Ye Z, Liu Z, et al. Ubiquitin ligase RNF20/40 facilitates spindle assembly and
- 542 promotes breast carcinogenesis through stabilizing motor protein Eg5. Nat Commun. Nature Publishing
- 543 Group; 2016;7:12648.

- 544 50. Nersesian S, Williams R, Newsted D, Shah K, Young S, Evans PA, et al. Effects of Modulating Actin
- 545 Dynamics on HER2 Cancer Cell Motility and Metastasis. Sci Rep. 2018;8:17243.
- 546 51. Walker S, Foster F, Wood A, Owens T, Brennan K, Streuli CH, et al. Oncogenic activation of FAK drives
- 547 apoptosis suppression in a 3D-culture model of breast cancer initiation. Oncotarget. 2016;7:70336–52.
- 548 52. Hamdan FH, Johnsen SA. DeltaNp63-dependent super enhancers define molecular identity in pancreatic
- 549 cancer by an interconnected transcription factor network. Proc Natl Acad Sci. 2018;115:E12343–52.

550

552 Figure legends

553

Fig.1: RNF40 and H2Bub1 are maintained in HER2-positive breast cancer. A-B: TMAs with primary mammary 554 555 carcinoma (n=178) and brain metastasis (n=78) lesions were stained for RNF40 and H2Bub1 by IHC. Distribution 556 of RNF40 and H2Bub1 staining intensity in all BCs (left panels) and in the HER2-positive subtype (right panel) in 557 primary tumors (A) and brain metastases (B). C) Representative pictures of low and high H2Bub1 and RNF40 558 staining intensity in primary HER2-positive BC specimens. D) Relapse-free survival plot (RFS) of HER2-positive 559 breast cancer patients with low and high gene expression of RNF40, using the online tool of kmplot.com. E) Disease-free survival of *Rnf40^{wt/wt}* compared to *Rnf40^{wt/fl}* or *Rnf40^{fl/fl}* mice. Logrank test. F) Bar graph depicting 560 561 the average number of observed tumors per animal in each transgenic mouse cohort. Student t-test. G) Tumor 562 growth kinetics of all transgenic mouse cohorts. H) Representative images of immunohistochemical staining of RNF40, H2Bub1 and HER2 in the *Rnf40^{wt/wt}* and *Rnf40^{fl/fl}* mammary carcinomas. Scale bar (white): 100 μm I) 563 564 Immunohistochemical detection of the Ki67 proliferation marker. Scale bars (white): 100 µm. **p-val<0.01, ***p-val<0.005. Error bars: standard error of the mean (SEM). 565

566

Fig.2: RNF40 loss impairs oncogenic properties of HER2-positive BC cells in vitro. A) Western blot validation of 567 568 RNF40 knockdown efficiency and decreased H2Bub1 levels in HCC1954 cells. B) Representative bright-field 569 pictures of control and RNF40 siRNA-transfected HCC1954 and SKBR3 cells. Scale bars (white): 500 μm. B and C: 570 Proliferation curves (C) and clonogenic assays (D) of control and RNF40-depleted HCC1954 and SKBR3 cells. 571 Quantification of the occupied area in clonogenic assays is shown for both cell lines (D, lower panel). Student t-572 test. E) Tumor sphere formation assay of control and RNF40-depleted HCC1954 cells (upper panel). 573 Quantification of the respective tumor spheres number normalized to the control condition (lower panel). 574 Student t-test. F) Representative pictures from immunofluorescence detection of RNF40 and the Ki67 575 proliferation marker in control and RNF40-depleted HCC1954 and SKBR3 cells. Scale bars (white) = 60 μ m (upper 576 panel). Quantification of the Ki67 immunofluorescence intensity of single nuclei in control and RNF40-depleted 577 HCC1954 and SKBR3 cells (lower panel). The median intensity values of the respective groups are provided as

578 green bars. Mann-Whitney test. **G)** Boyden-chamber-based migration assay of control and RNF40-depleted 579 HCC1954 cells with representative results (upper panel) and the corresponding quantification (lower panel). *p-580 val<0.05, **p-val<0.01, ***p-val<0.005. Error bars of all quantification analyses: SEM.

581

582 Fig.3: RNF40 loss increases apoptosis and impairs the expression of key components of the actin regulatory pathway in HER2-positive BC cells. A) Western blot analysis of the total and phosphorylated forms of ERK1/2 583 584 and AKT in control and RNF40-depleted HCC1954 cells. 1 µM Lapatinib (lap) was applied for 12 hours as a 585 positive control. B) Volcano plot displaying gene expression changes occurring in HCC1954 cells upon RNF40 586 depletion and measured by mRNA sequencing. C) Gene Set Enrichment Analysis (GSEA) of the mRNA sequencing 587 data significantly enriched for "Hallmark Apoptosis" geneset enriched in the RNF40-depleted condition. D) 588 Western blot analysis showing that the markers of apoptosis, the cleaved forms of caspase 3 and PARP, are at 589 higher levels in RNF40-depleted HCC1954 cells compared to the control condition. E) Annexin V assay of control 590 and RNF40-depleted HCC1954 cells. F) Pathway enrichment analysis (EnrichR web tool) showing that genes 591 significantly downregulated upon RNF40 knockdown are enriched for the KEGG 2019 signature "Regulation of actin cytoskeleton". A heatmap depicting the differential expression of genes involved in this signature is 592 593 provided in the right panel). G-H: The identified signature was validated via qRT-PCR (G) and western blot (H) for 594 selected genes in HCC1954 cells. Student t-test. *p-val<0.05, **p-val<0.01, ***p-val<0.005. Error bars of all 595 quantification analyses: SEM.

596

Fig.4: RNF40 controls the actin regulatory pathway to sustain the viability of HER2-positive BC cells *in vitro* and *in vivo*. A) Western blot analysis showing a reduction of phosphorylated cofilin (p-cofilin) upon RNF40 knockdown and ROCK inhibitor treatment (RKI-1447) in HCC1954 cells. B) Western blot analysis showing a reduction of phosphorylated cofilin in VAV3-depleted HCC1954 cells. C) Representative pictures of immunofluorescence staining for F-actin in control, RNF40-depleted and RKI-1447-treated (ROCK inhibitor) HCC1954 cells (right panel). Quantification of F-actin intensity in the respective conditions (left panel). Scale bars

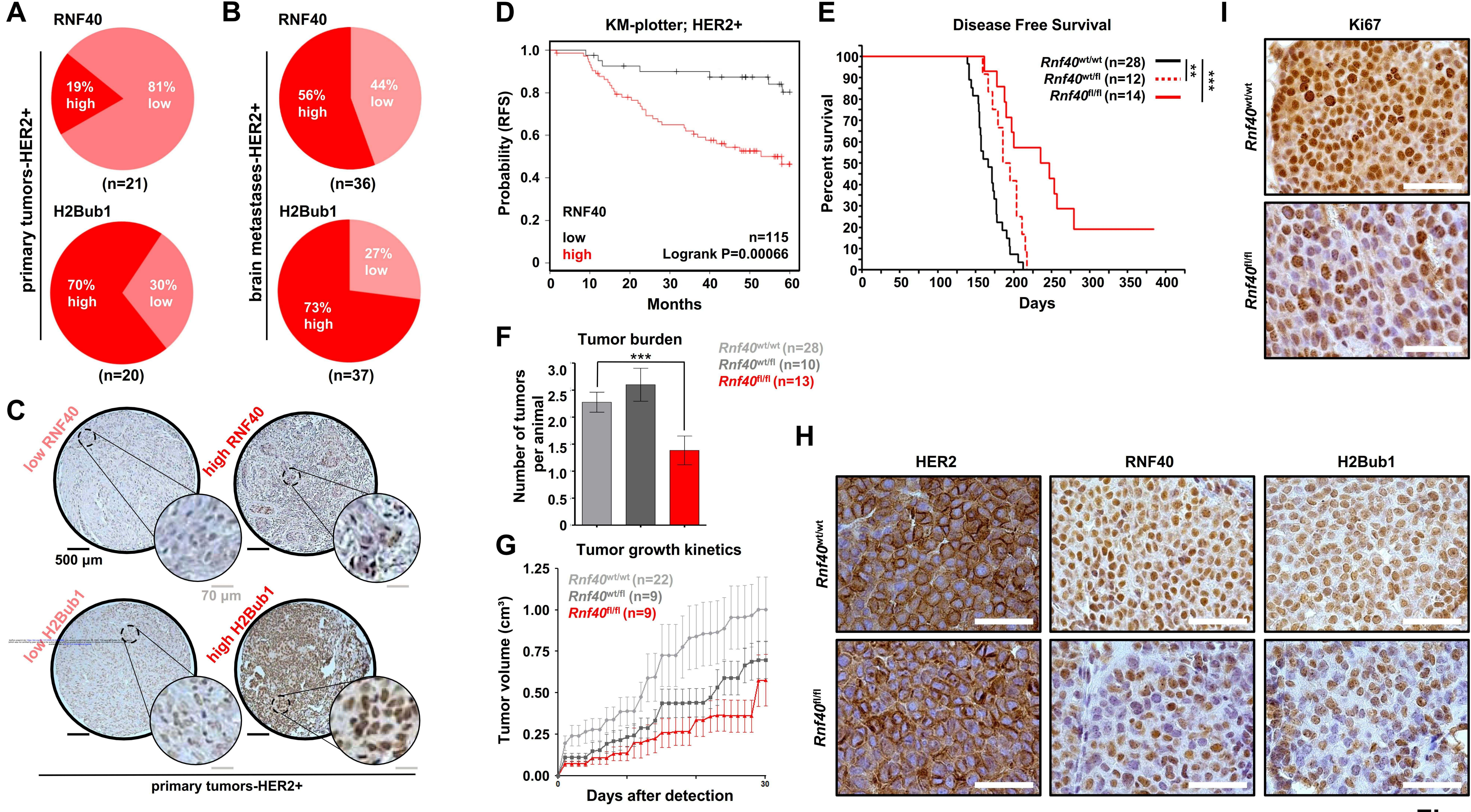
(white) = 50 µm. Mann-Whitney test. D) Representative pictures of p-cofilin detected by immunofluorescence in 603 the murine *Rnf40*^{wt/wt} and *Rnf40*^{fl/fl} tumors. Western blot analysis assessing cleaved PARP and cleaved caspase 3 604 605 levels (cl: cleaved, fl: full length) (E) or phosphorylated and total FAK (F) in control, RNF40-depleted and RKI-606 1447-treated HCC1954 cells. G) Representative immunofluorescence pictures of vinculin in control, RNF40-607 depleted and VAV3-depleted HCC1954 cells (right panel). Bar graph displaying the median focal adhesion area in 608 the respective conditions (left panel). Scale bars (white) = 50 μ m. Mann-Whitney test. H-I) Annexin V assay (H) 609 and proliferation assay (I) of control and RNF40-depleted HCC1954 cells with and without the S1PR, agonist 610 CYM-5441. Quantification of cell confluency (right panel). Student t-test. *p-val<0.05, **p-val<0.01, ***p-611 val<0.005. Error bars of all quantification analyses: SEM.

612

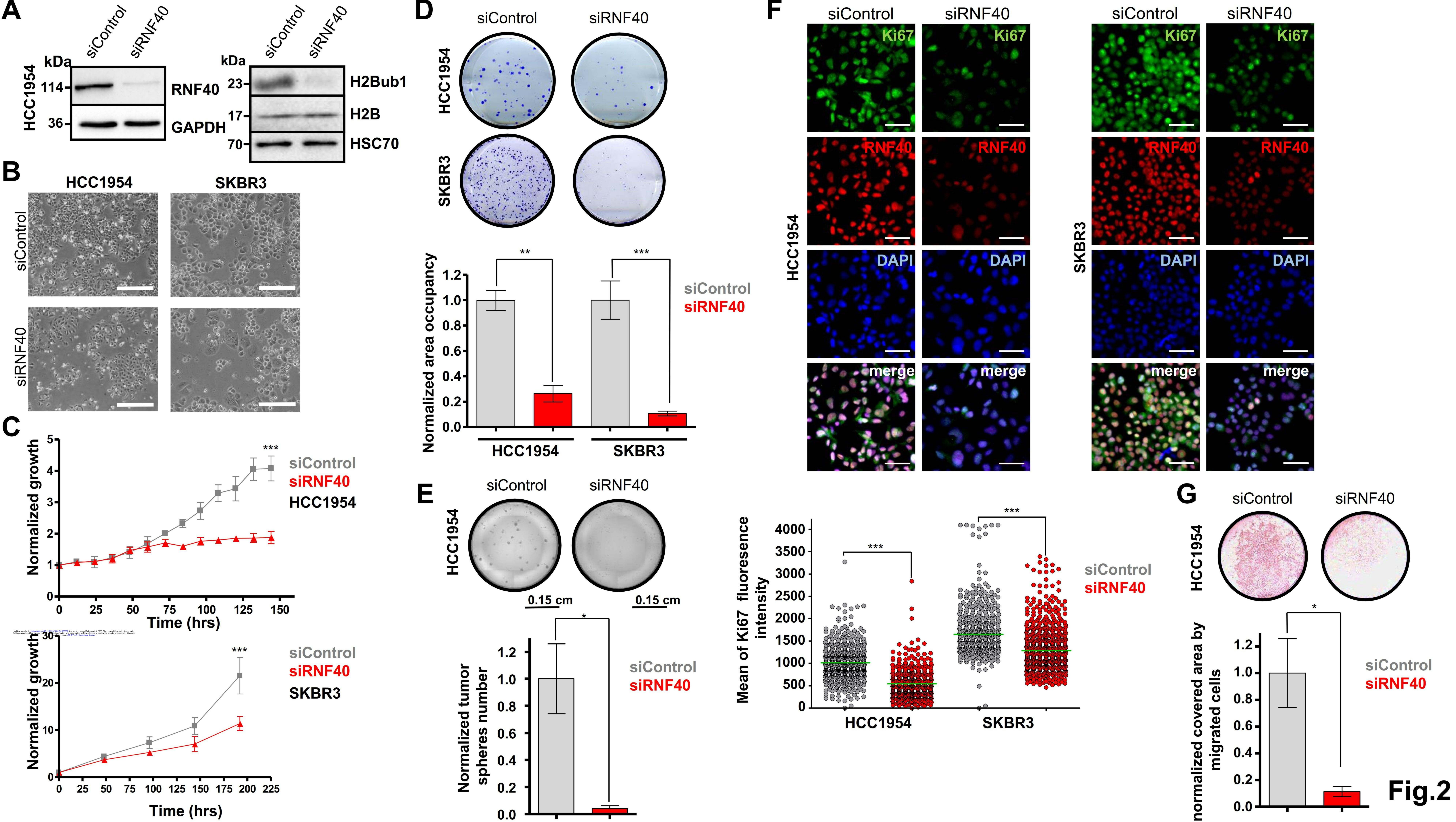
613 Fig.5: RNF40 regulates gene expression of important members of the RHO-ROCK axis in an H2Bub1/H3K4me3-614 dependent manner. A) Gene body H2Bub1 occupancy profiles on down-, up- and unregulated genes upon 615 RNF40 depletion (regulated genes |log2FC|≥0.6, p-val<0.05, unregulated genes |log2FC|≤0.1, p-val>0.95). B) 616 Schematic workflow showing the procedure utilized to identify regions losing or gaining H3K4me3 occupancy upon RNF40 depletion. C) Differential Binding Analysis results showing H3K4me3 regulated ($|log2FC| \ge 0.7$, 617 618 FDR<0.05) and unregulated regions (in purple). D) Heatmaps and respective aggregate profiles depicting 619 changes of H3K4me3 occupancy in the identified gained (log2FC≥0.7, FDR<0.05, peak concentration≥6.2), lost 620 peak concentration \geq 6.2) or unregulated ($|\log 2FC| \leq 0.2$, FDR>0.1, (log2FC≤-0.7, FDR<0.05, peak 621 concentration≥6.2) regions upon RNF40 depletion based on the DiffBind analysis results in C. E) Aggregate plots 622 showing changes of H3K4me3 occupancy at TSS-associated regions of genes identified in RNA-seq analysis as 623 robustly down-, up- (|log2FC|≥0.8, p-val<0.05) and unregulated (|log2FC|≤0.1, p-val>0.95) following RNF40 624 depletion. F) Quantification of changes in H3K4me3 peak width upon RNF40 depletion in regulated and 625 unregulated genes. G) Left panel: classification of genes influenced by RNF40 depletion into Group A 626 (simultaneous downregulation and H3K4me3 loss at TSS region), Group B (downregulation without H3K4me3 627 loss) and Group C (H3K4me3 loss at TSS region without expression changes). Right Panel: Group A genes were

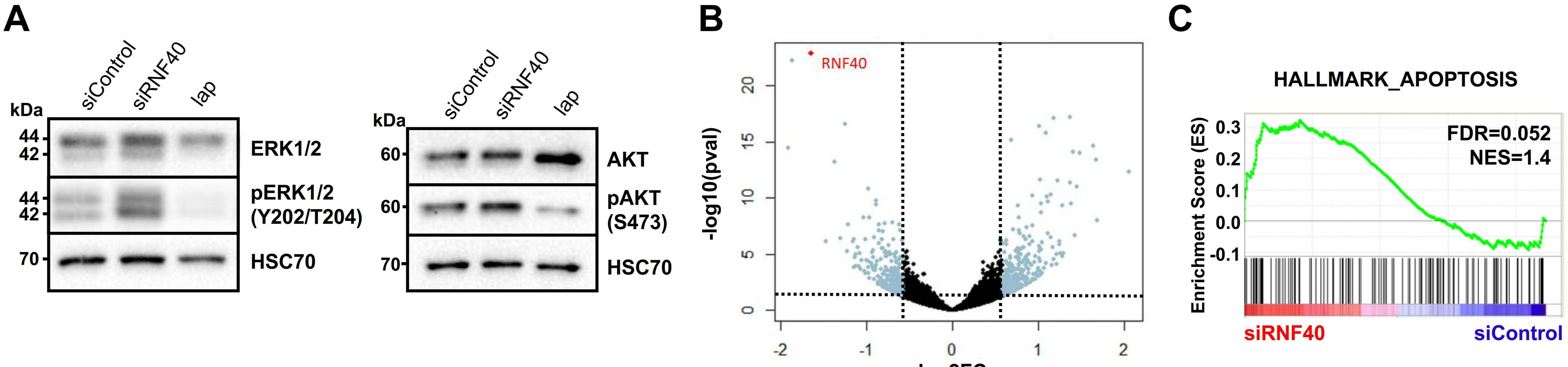
628	analyzed for pathway enrichment using the online EnrichR web tool (https://amp.pharm.mssm.edu/Enrichr3/).
629	H) Box-Whiskers plot providing the median of normalized counts of the three gene groups (Group A, B and C). I)
630	Changes in H3K4me3 occupancy at TSS-associated regions of group A, B and C genes. J) Aggregate plots of
631	H2Bub1, H3K79me2, H3K36me3, H3K27ac, H3K9ac or RNApol II occupancy at TSS of group A, B and C genes in
632	control HCC1954 cells (Accession number: GSE85158, GSE72956). All statistical tests: Mann-Whitney Test. **p-
633	val<0.01, ***p-val<0.005.
634	
635	Fig.6: RNF40 enacts a tumor supportive role in HER2-driven mammary carcinoma via controlling the
636	RHO/ROCK-dependent actin regulatory axis. RNF40-driven H2B monoubiquitination is essential for

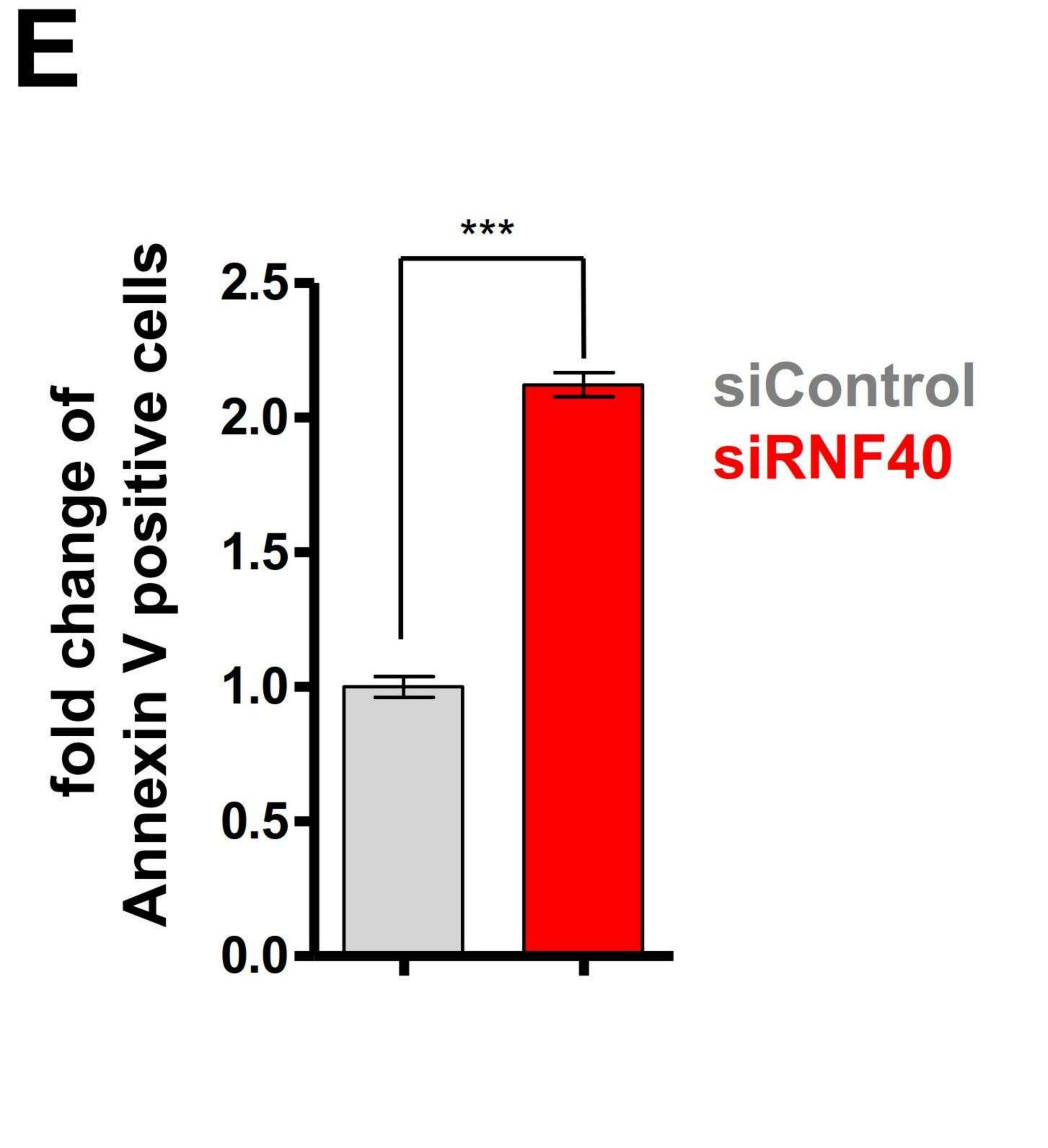
637 transcriptional activation of the RHO/ROCK/LIMK pathway components and for proper actin polymerization via a 638 trans-histone crosstalk of histone 3 lysine 4 trimethylation (H3K4me3). Loss of RNF40 expression leads to the 639 impairment of the H2Bub1-H3K4me3 axis, thereby dysregulating the actin dynamics and disrupting the focal 640 adhesions (FA) and their pro-survival activity via FAK in HER2-positive breast cancer cells.

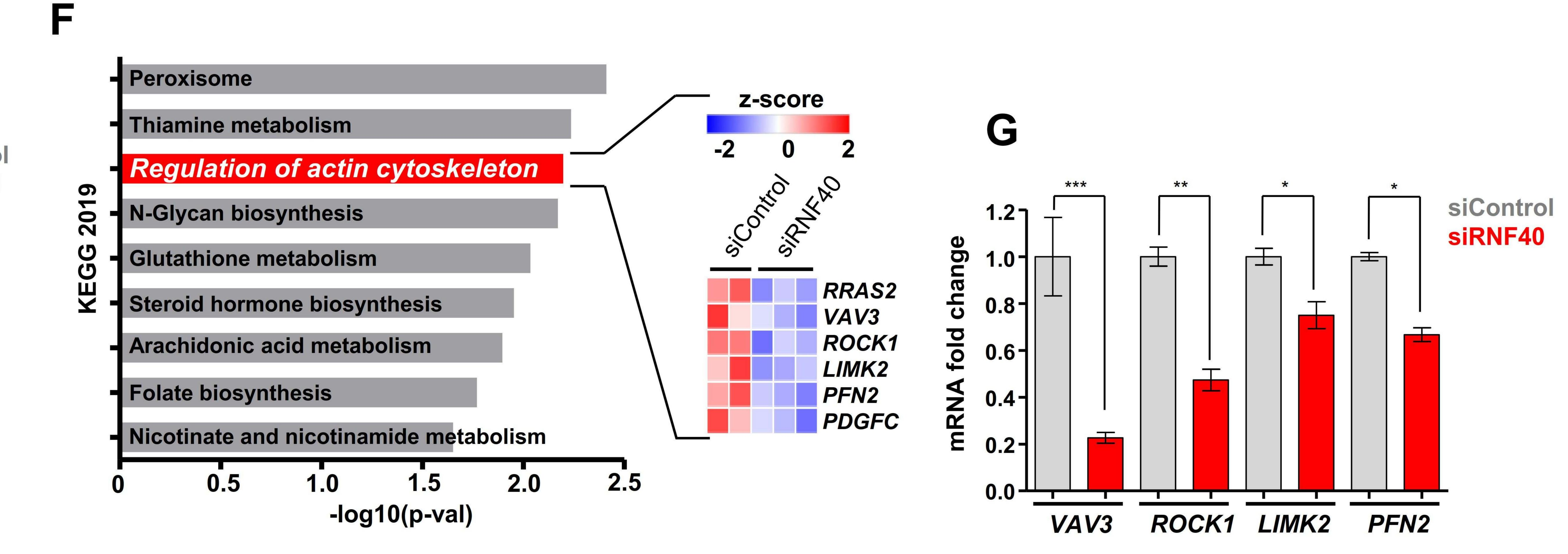




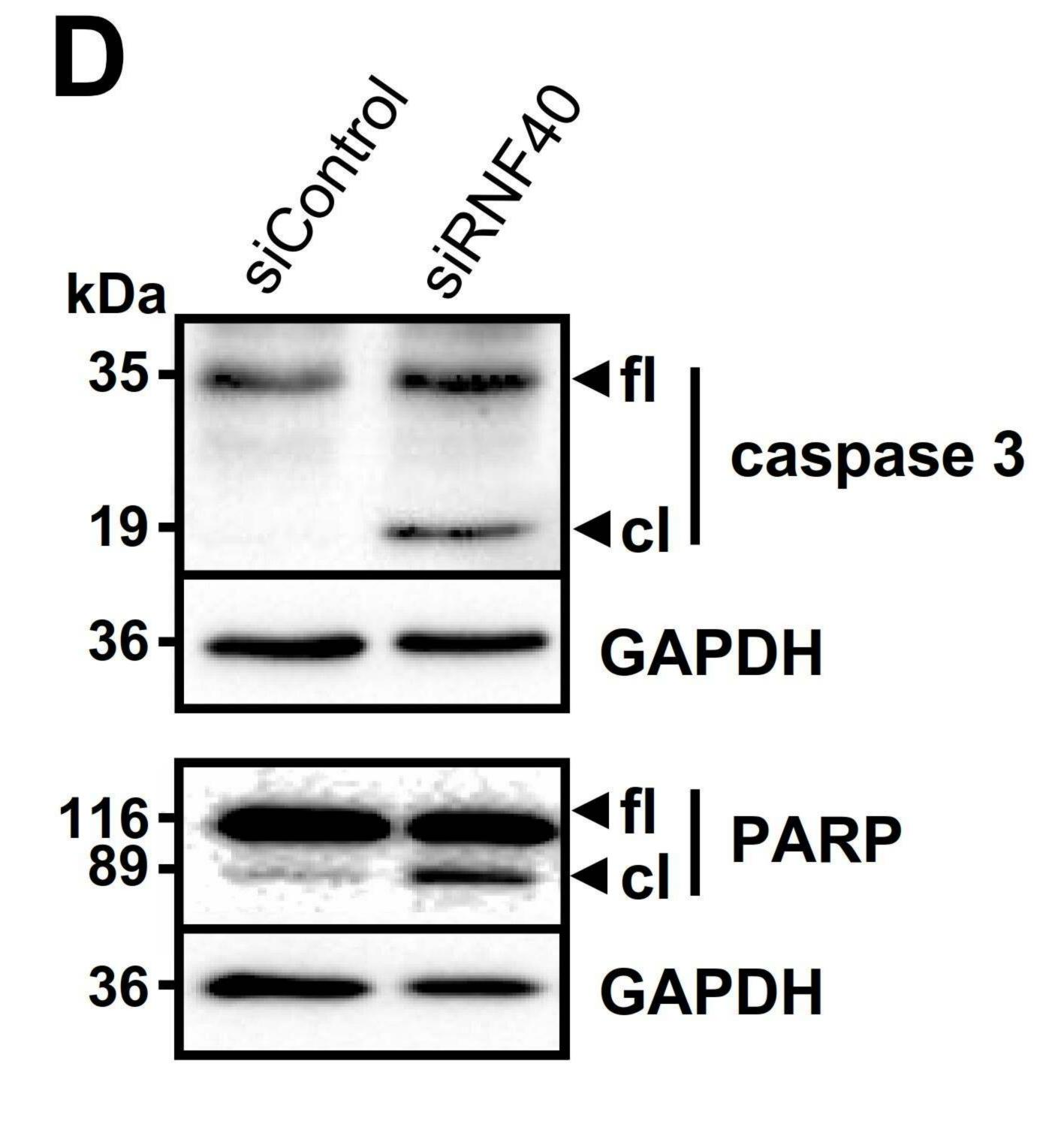












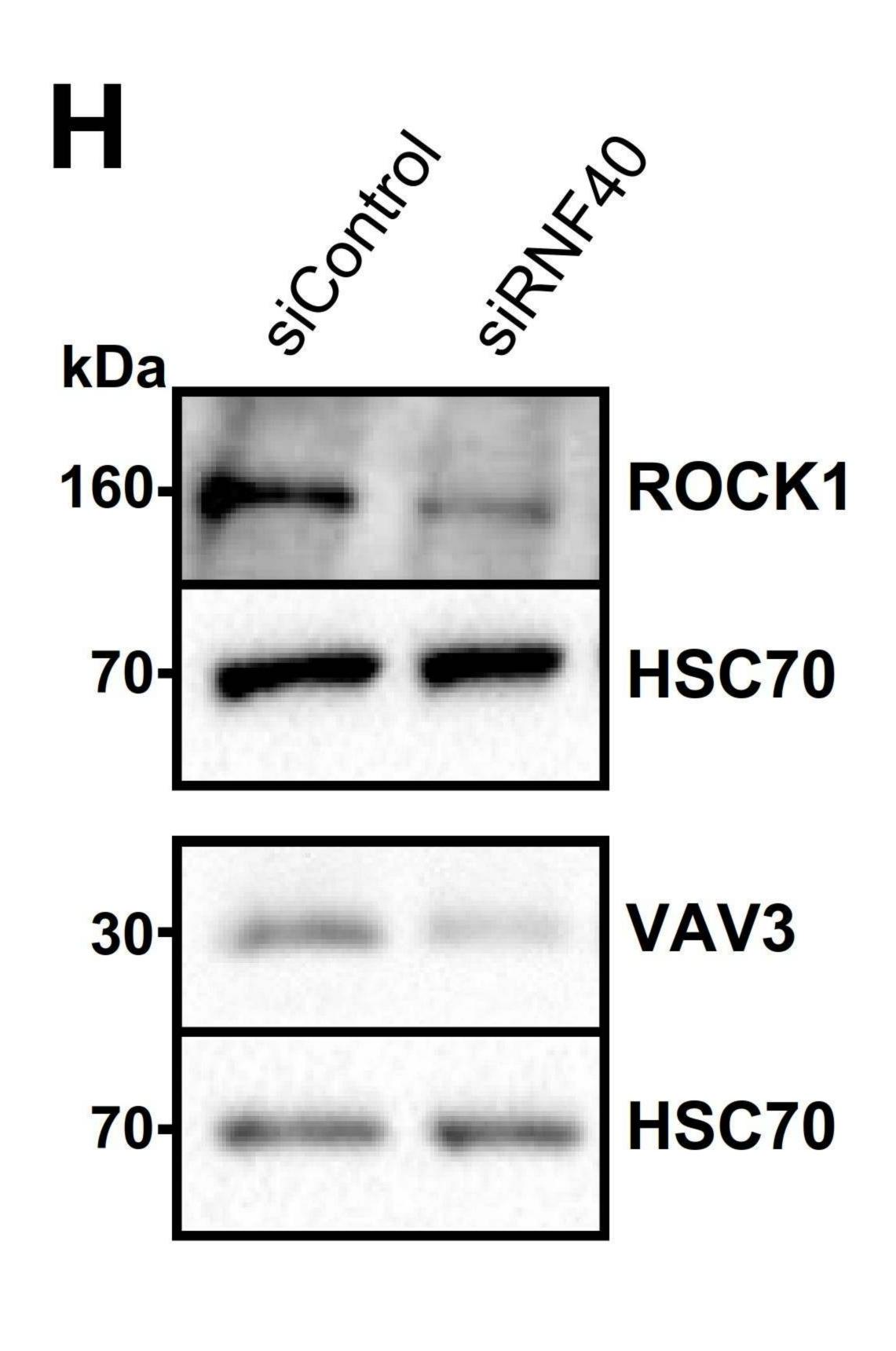
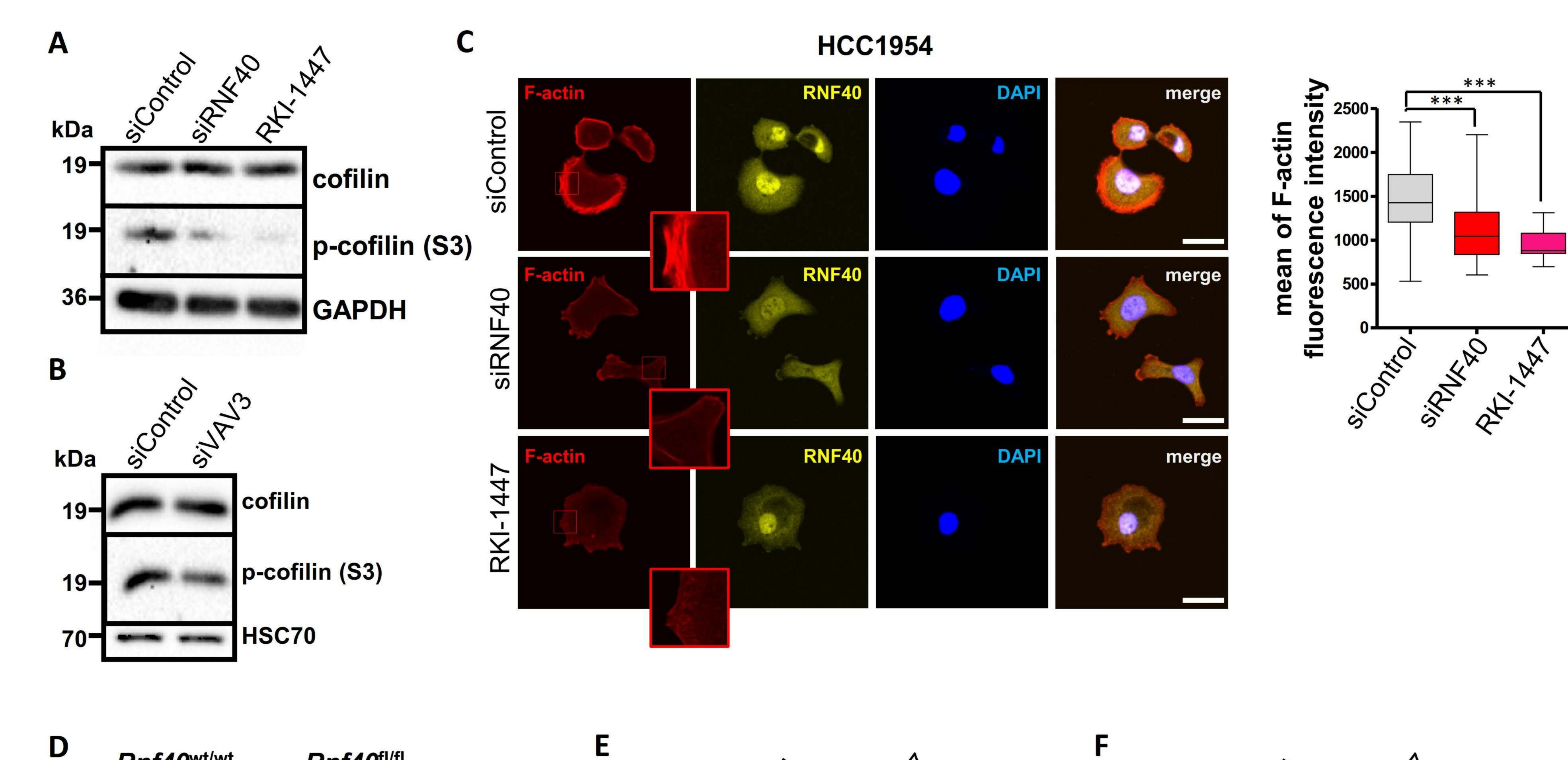


Fig.3



D Rnf40^{fl/fl} Rnf40^{wt/wt}

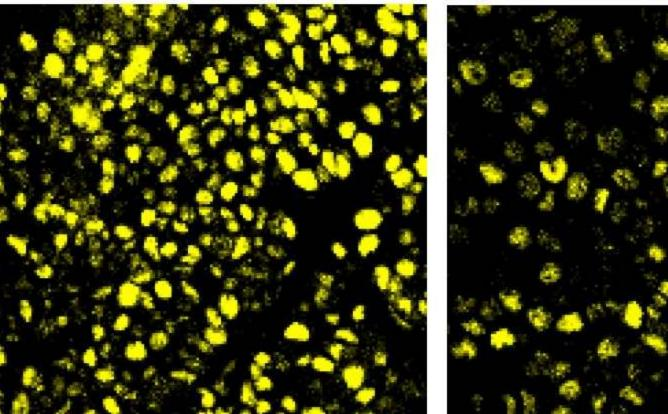


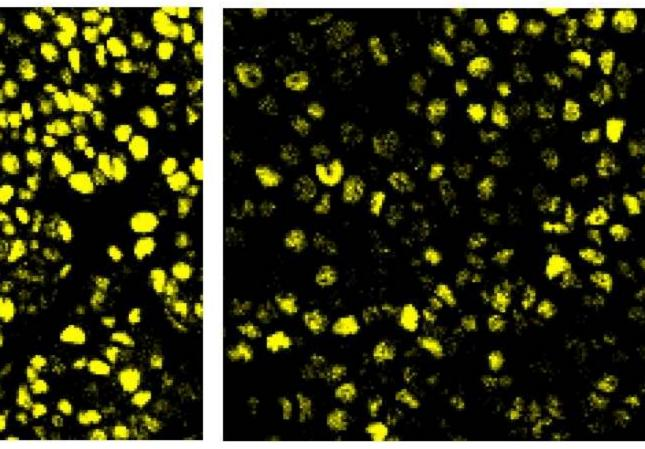


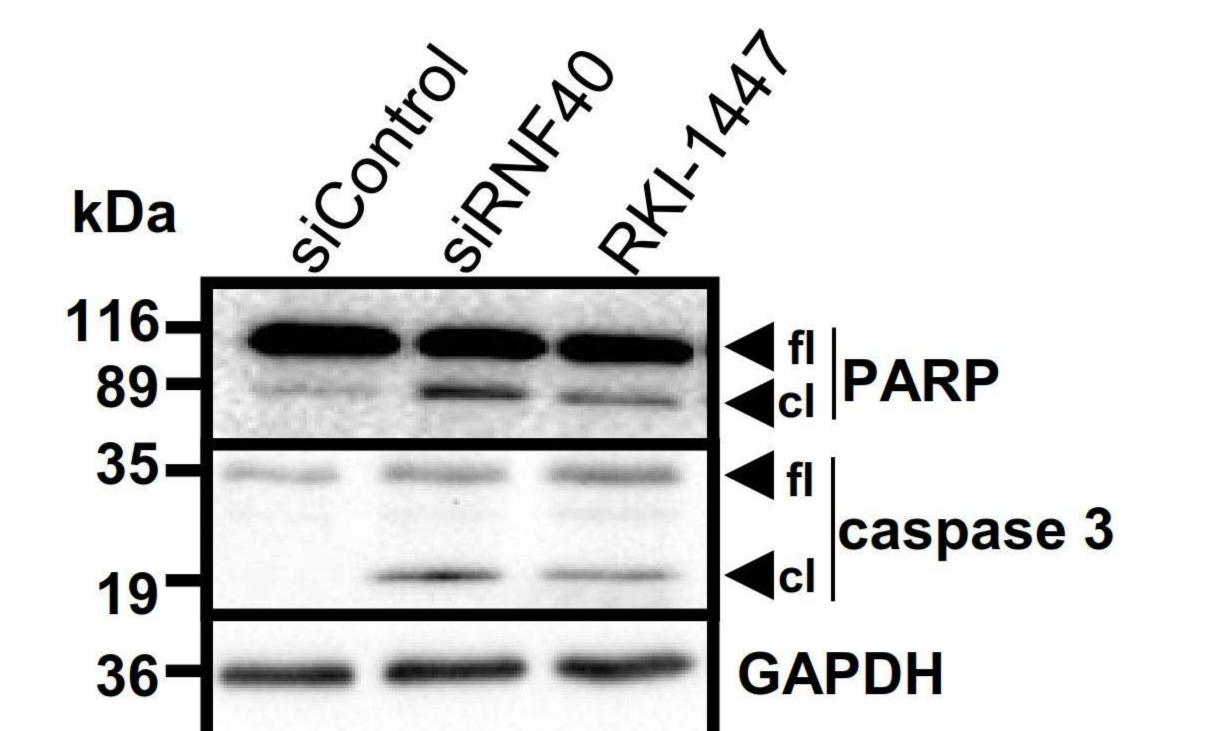


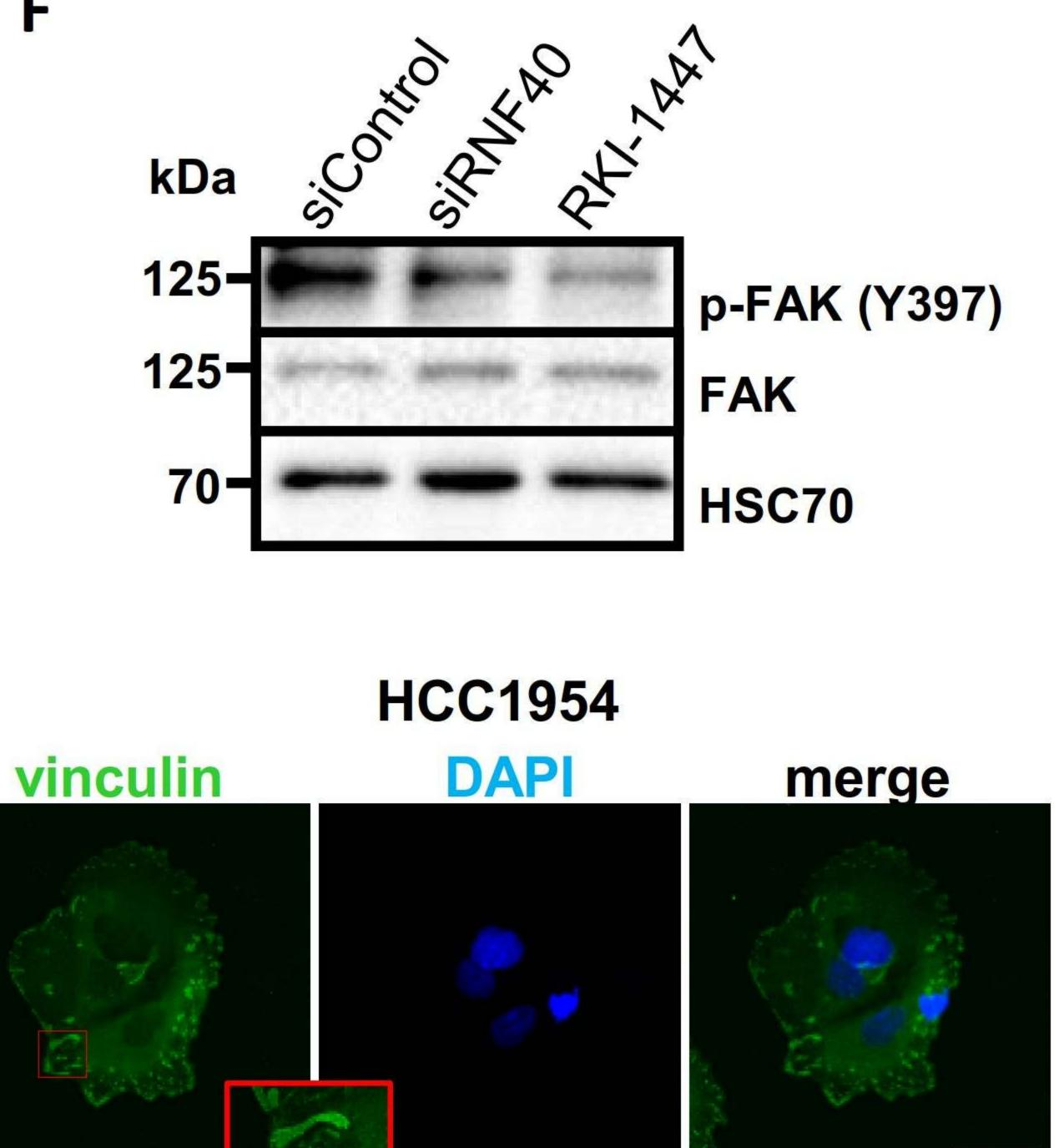


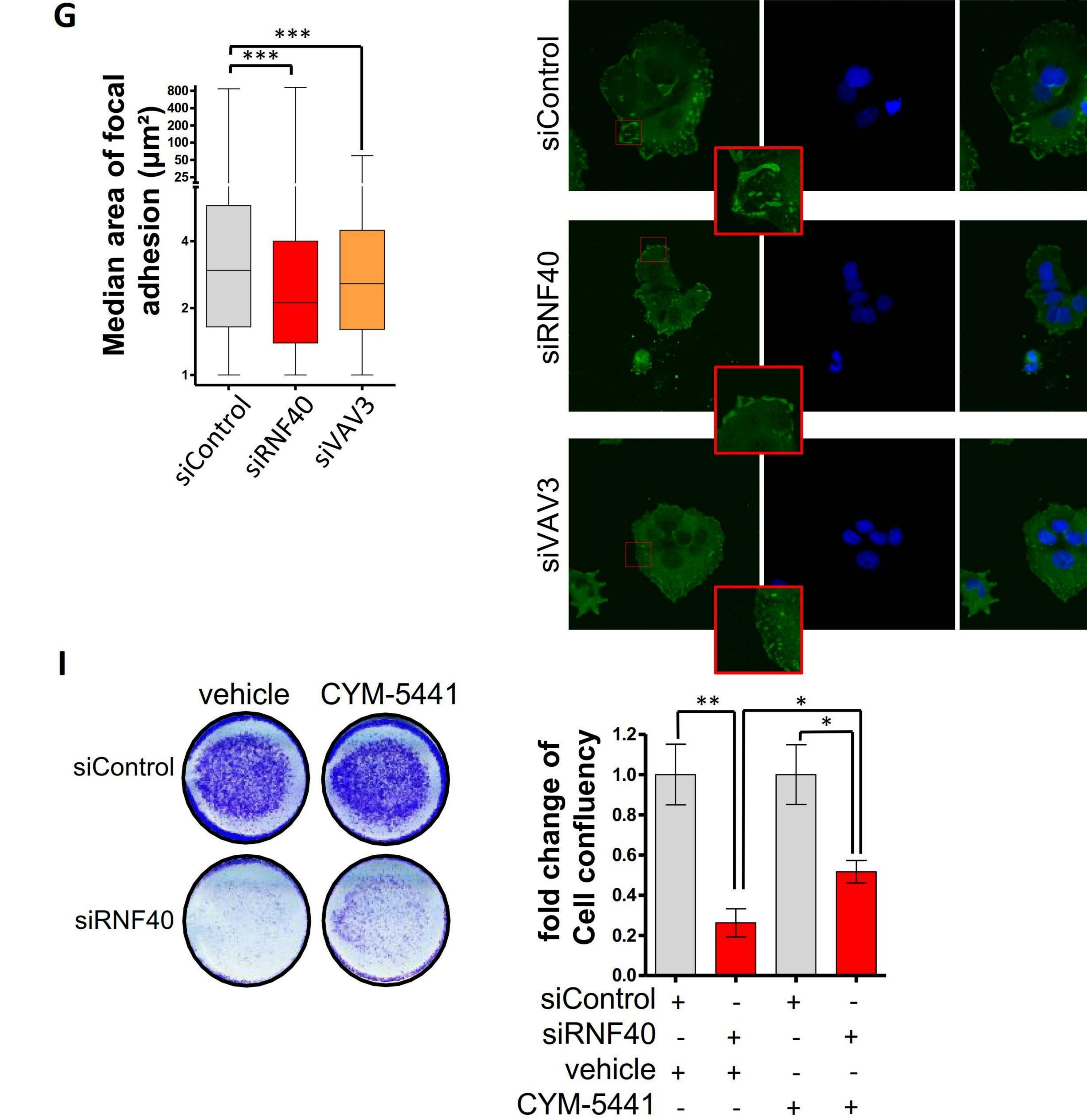
H2Bub1

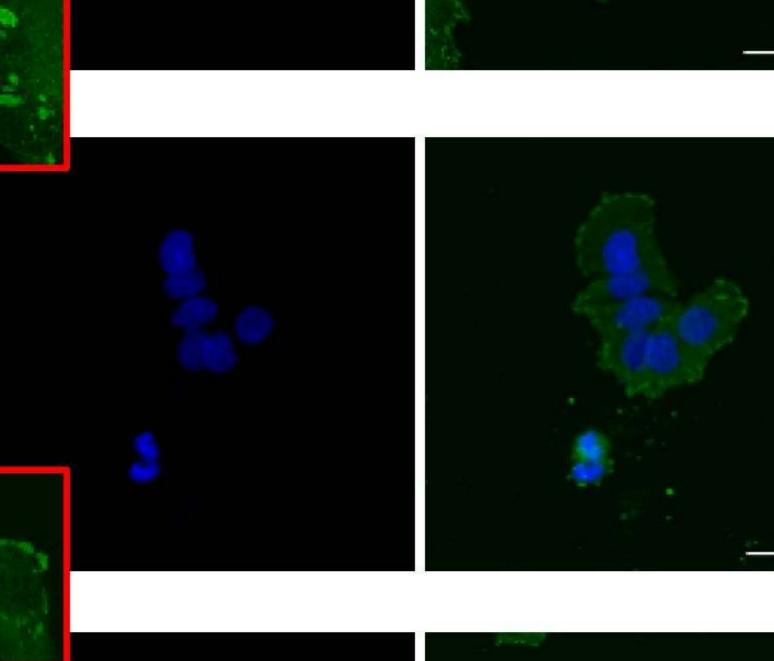


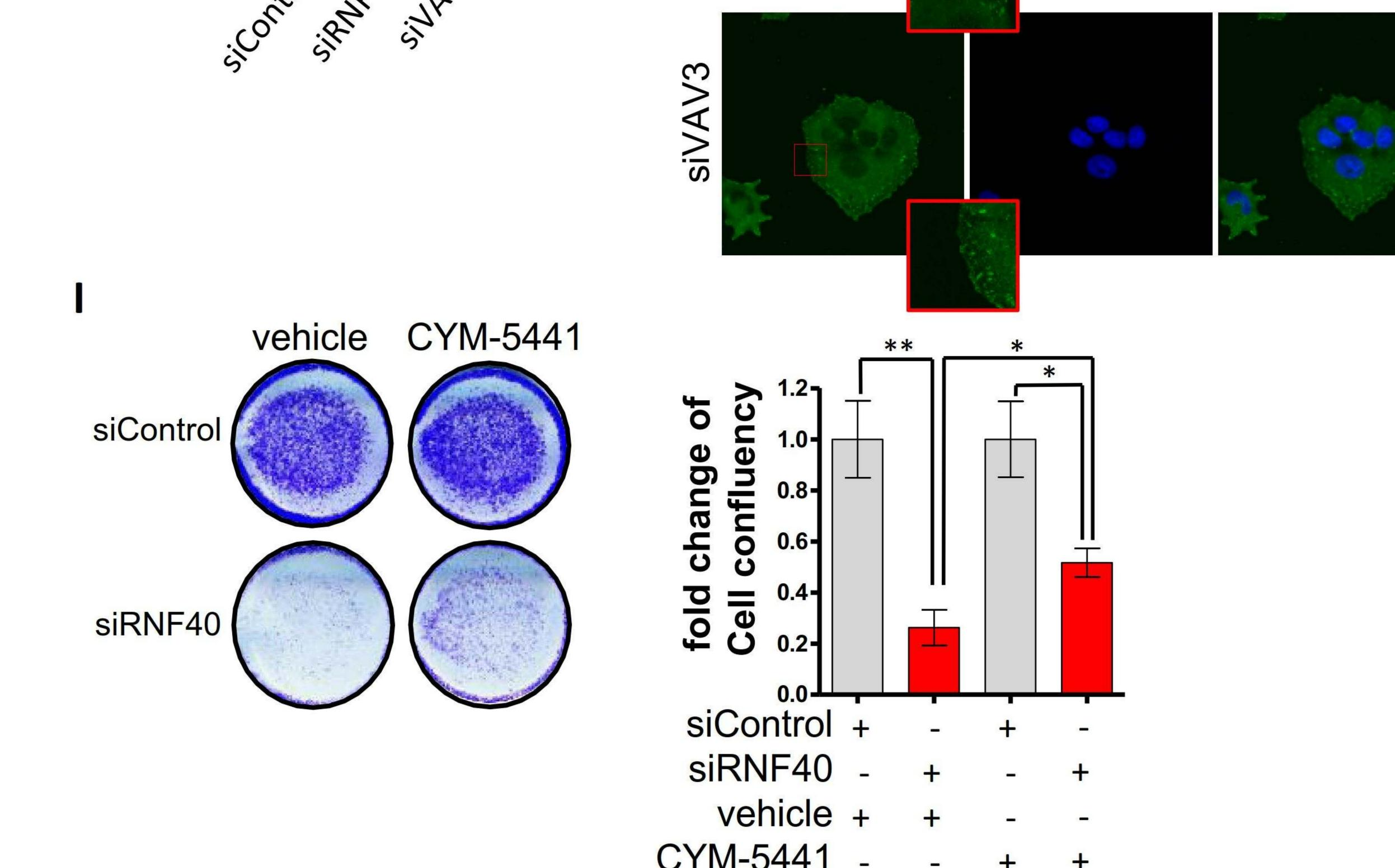












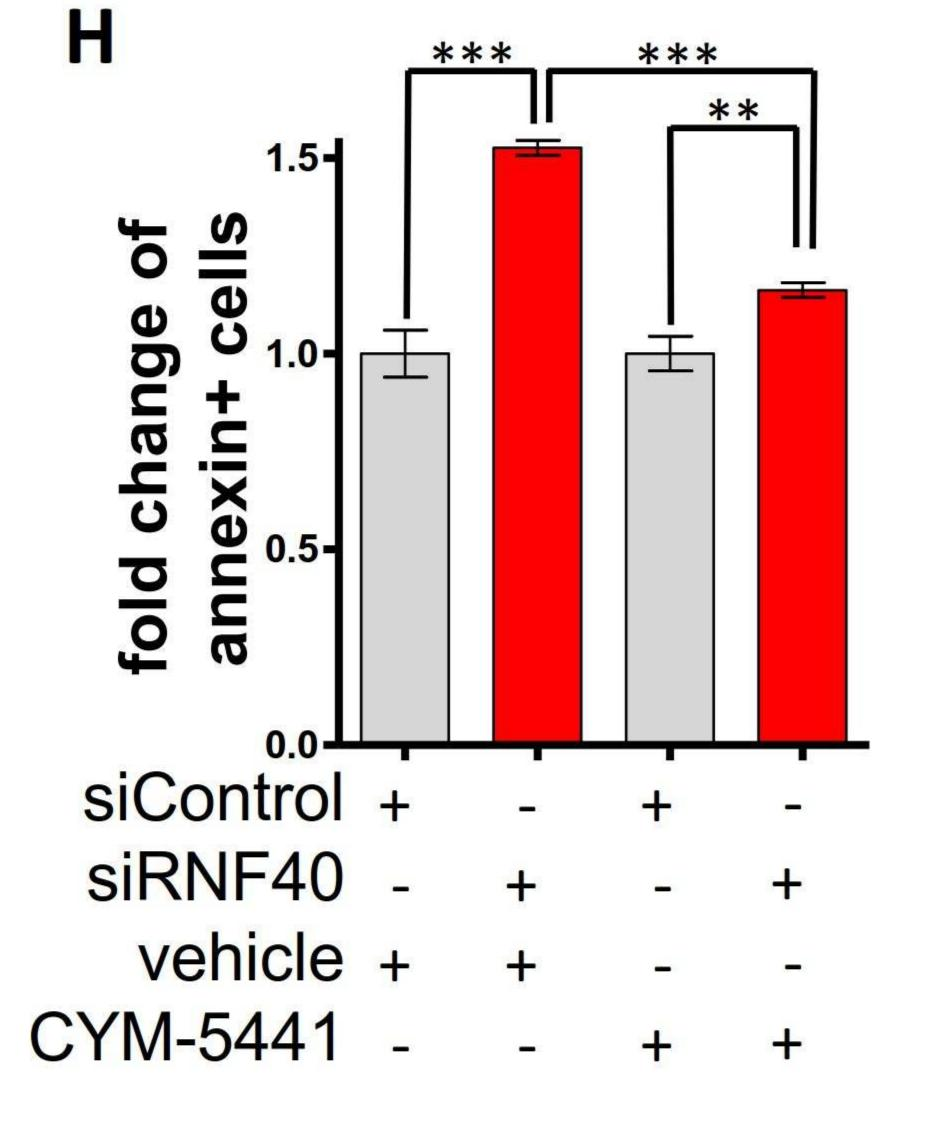


Fig.4

bioRxiv preprint doi: https://doi.org/10.1101/2020.02.24.962902; this version posted February 25, 2020. The copyright holder for this preprint (which was not certified by peer review) is the author/funder, who has granted bioRxiv a license to display the preprint in perpetuity. It is made

available under aCC-BY 4.0 International license.

